Ref. Ares(2019)7880741 - 20/12/2019

Grant No.: 641073

Bio-HyPP

Deliverable No	Title	Submission Due Date	WP/Lead
D1.7	System performance and dynamic models validation	31.12.2019	WP 1 / DLR

Short Summary	This document describes the deliverable D1.7 "System performance and dynamic models validation". Thermodynamic performance models for the top-economic layout and for the top-performance layout have been developed. Their validation is described in this document. Additionally, dynamic models for the top-economic layout, a real-time model for the emulation of the SOFC and a dynamic model of this emulation model have been developed and used for further simulations.
Author/Corresponding author(s)	DLR: Thomas Krummrein, Melanie Herbst, Marius Tomberg - UNIGE: Mario L. Ferrari, Luca Mantelli, Andrea Giugno
Printed Date	20.12.2019

Dissemination Level		
PU	Public	X
PP	Restricted to other programme participants (including the Commission Services)	
RE	Restricted to a group specified by the consortium (including the Commission Services)	
CO	Confidential, only for members of the consortium (including the Commission Services)	

Table of Contents

Table of Figures

Table of Tables

List of Acronyms

AC	alternate current
AN	anode
ANOVA	analysis of variance
APH	air pre-heater
ASR	area specific resistance
ave	average
C	compressor
CA	cathode
CBV	cold bypass valve
CCM	main combustor for SOFC emulation
CCF	central composite design face centred
CCS	start-up combustor
CH_4	methane
DLR	Deutsches Zentrum für Luft- und Raumfahrt e.V. (German Aerospace Center)
FC	fuel cell
FLOX®	flameless oxidation
FPH	fuel pre heater
HyPP	Hybrid power plant
in	inlet
IRR	internal rate of return
max	maximum
MGT	micro gas turbine
MGT test rig	Hybrid power plant test rig consisting of real MGT and emulated SOFC
NG	natural gas
OGB	off-gas burner
OP	Operation point
out	outlet
PDF	probability density function
PID	proportional integral derivative
REC	recuperator
REF	reformer
RS	response surfaces
SOFC	solid oxide fuel cell
SOFC test rig	Hybrid power plant test rig consisting of real SOFC and emulated MGT
T	turbine
TC	turbocharger
UNIGE	University of Genoa
VBE	bleed valve

WGV	wastegate valve
WP	work package

Variables

A	area
A_{eff}	effective cross section area
C	cost
CFN	annual cash flow
COV	coefficient of variance
EOF	end of life
EOH	equivalent operating hours
F, RR	recirculation ratio
FO	fractional opening
I	current
IRR	internal rate of return
J	current density
K_{ohm}	ohmic loss coefficient
m	mass flow rate
m_p	reduced mass flow of turbomachinery
N_p	reduced shaft speed of turbomachinery
P	power
p	pressure
S	section
S/C	steam-to-carbon ratio
T	temperature
TIT	turbine inlet temperature
TOT	turbine outlet temperature
U_f	fuel utilization factor
Ucell	SOFC cell voltage
V	voltage
Vr	blade-to-jet velocity
W	Watt
w	mass concentration
x	distance
η	efficiency
Π	pressure ratio
Φ	flow coefficient

Subscripts

amb	ambient
c	compressor
cell	fuel cell
diff	diffuser
ej	ejector
el	electrical
is	isentropic
maint	maintenance
prim	primary duct
rec	recuperator
sec, 2	secondary duct
t	turbine
0	reference

1 Introduction [author: DLR: Melanie Herbst]

The aim of the Bio-HyPP project has been the development of a hybrid power plant [28] – a combination of solid oxide fuel cells (SOFC) and a micro gas turbine (MGT). For this development, the understanding of both the characteristics of the MGT system and its components as well as the characteristics of the SOFC system and its components are essential. Therefore, two separate test rigs have been set up as a part of WP4: the MGT hybrid power plant test rig (real MGT with emulated SOFC) and the SOFC hybrid power plant test rig (real SOFC with emulated MGT) [25].

For setting up the test rigs, thermodynamic performance models have been developed and used in the beginning of the project. A thermodynamic performance model for the top-performance layout (DLR) and a model for the top-economic layout (UNIGE) have been developed. Within the course of the project, dynamic and real-time models have been developed additionally.

This deliverable (D1.7) describes the models and their validation with experimental data. It is subdivided into six chapters.

Chapter 2 describes the system layout and the model of the top economic layout. The model validation and also additional simulation results are described.

In Chapter 3 the validation of the top-performance model is described. This chapter refers to a former deliverable D1.2 which described the model and the plant layout.

Chapter 4 describes a dynamic model for the top-economic layout. After model validation, simulation results are shown and described leading to insights about the control possibilities.

Chapter 5 describes the real-time model used for SOFC emulation in the top-economic layout.

Chapter 6 describes an additional model of the SOFC emulator. It is described how this has been used to set the control to avoid critical conditions.

In chapter 7 the conclusions are presented.

2 Thermodynamic Performance Modelling of top-economic layout [author: UNIGE: Mario L. Ferrari, Luca Mantelli, Andrea Giugno]

This section regards the modelling activity performed by UNIGE for the thermodynamic analysis of the "top economic" layout (the turbocharged SOFC). Different steady-state conditions have been considered to calculate the plant performance in wide operative ranges.

2.1 System layout

The turbocharged SOFC system "top economic layout" is based on the coupling of a fuel cell stack with a turbocharger. Therefore, this layout is able to couple the cost benefit of a mass production turbomachinery with the efficiency increase related to the SOFC pressurization (about +11% efficiency increasing the SOFC pressure from 1 bar to 5 bar [1]). If compared to a micro gas turbine hybrid system, the power is lower (10%-15%) due to the turbocharger application. Nevertheless, this design choice is motivated by the cost reduction of the turbomachine: few hundreds of euro (price for the largest turbochargers) instead of more than one thousand of €/kW (price for micro gas turbines) [2][3][4].

As shown in the system layout (Figure 1), the compressed air flow rate is pre-heated by the recuperator (recovering a part of the exhaust thermal content) and diverted to the SOFC system. Then, after a further pre-heating, the air flow duct is connected to the SOFC cathode inlet. On the fuel side (where biogases of different compositions are considered), a pre-heating is performed using a small amount of the system exhausts upstream of the anodic ejector. This component is necessary to generate an anodic recirculation for providing both thermal content and steam flow for the reforming reactions. Since during all operative conditions it is necessary to avoid carbon deposition in the anodic loop, the ejector needs to be sized properly, as discussed in previous works [5][6]. The ejector outlet duct is connected to the reformer inlet, upstream of the SOFC anodic side. The flows discharged by the cathodic side and the anodic loop are mixed in the Off-Gas Burner (OGB) where the fuel not converted in the SOFC is burned. The OGB outlet flow is used for pre-heating the cathodic side and to supply the necessary heat to the reformer, upstream of the turbine of the turbocharger generating the power necessary for the compressor. Finally, the turbine outlet flow is used in the hot side of the recuperator and the fuel pre-heating heat exchanger.

Moreover, Figure 1 shows additional pipe lines (bleed, recirculation, bypass and wastegate) equipped with control valves. These devices are necessary to control the system, satisfying all the constraints in both design and off-design conditions (including the fuel composition change). In detail, the bleed valve is used to prevent compressor surge and to control the cathode inlet temperature, while the wastegate is used to avoid turbocharger over-speed. Moreover, the recirculation line generates higher temperature values at the compressor inlet,

and the bypass valve is able to manage the cathodic air flow (and, as a consequence, the SOFC temperature) [7].

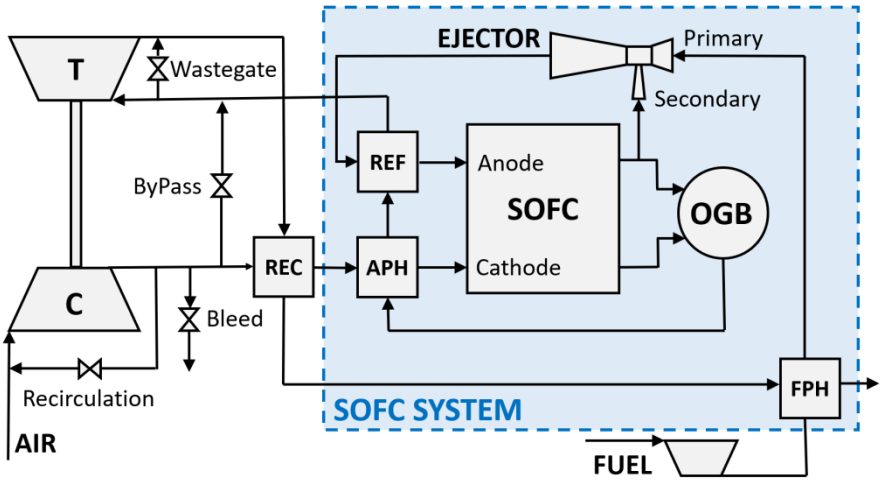

Figure 1: Plant layout of the top-economic layout

2.2 Model description

The model has been implemented based on component tools available in Matlab®-Simulink® considering a 30 kW size system. Global inlet-outlet balances (mass and energy equations) have been considered for all the components. The Off-Gas Burner (OGB) and the anodic ejector models are based on a 0-D approach. Instead, the SOFC, the reformer and the heat exchangers are simulated using 1-D models to correctly evaluate the not-negligible property distributions [8][9]. All the component tools were based on the following hypotheses: (I) air composed of nitrogen, oxygen, water, carbon dioxide and argon, (II) anodic flow including only the most significant species (methane, carbon monoxide, carbon dioxide, hydrogen, nitrogen and water), (III) equilibrium conditions for reforming and shifting reactions, and (IV) electrochemical reactions of carbon monoxide and methane considered negligible. The SOFC model takes into account the thermal losses of the fuel cell, while the other components external surfaces are considered adiabatic.

The SOFC model has been implemented considering 10 finite elements with the calculation of Nernst's, losses and energy equations as in the following steps: (a) the consumed hydrogen is known from the current, (b) product/reactant balance is used to evaluate the chemical composition, (c) energy equation to evaluate the temperature, (d) real voltage obtained from Nernst's potential and the losses (activation, Ohmic and mass transfer). More details related to the SOFC model equations and assumptions are described in [7][10].

For the other components, the following additional assumptions have been considered:

- equilibrium conditions for reforming and shifting reactions (reformer);

- mass, momentum and energy global equations, necessary to calculate the recirculation on the basis of the Venturi effect [11] (ejector);
- calculation based on constant isentropic efficiency (fuel compressor);
- heat exchangers performance based on the convection and conduction heat exchange equations (REC, APH and FPH);
- interpolation of the performance maps (compressor and expander of the turbocharger);
- constant coefficient for mechanical losses (turbocharger shaft).

A further detail has to be discussed for the turbocharger model considering that standard maps were implemented because commercial turbochargers were considered not optimized for such SOFC application (see D.1.5). Moreover, these maps were scaled in agreement with the fuel cell requirements. Since it is necessary to couple the compressor with a larger turbine (not available matching considering the automotive applications), a preliminary analysis was able to show an optimal map combination for compressor and turbine.

2.3 Model validation

The model of each plant component was validated against experimental data in different previous works [8][9][10][11][13]. Reformer and SOFC tools have been validated mainly in [8] and [9]. In [8] these models were validated comparing simulations results against experimental data collected running a Staxera GmbH SOFC system. These data included measurements of temperature, flow rate, pressure drop and electrical power. The calibration of the models was performed referring to the design operating conditions. To validate models, different operating conditions, with different values of power output, have been considered. The validation of the SOFC is performed comparing the values voltage, current density and temperature. In Figure 2 the validation of the temperature distribution along the cell is shown for three different conditions, A, B and C, characterized by low, medium and high current densities respectively. Model results show that temperature profiles are almost uniform for condition A, while a marked temperature increase along x-coordinate is visible at conditions B and C. This can be explained observing that, when the electrical current increases, even if the electrical power released increases as well, the main effect is an increase of the heat dissipation along the cell. This is the cause for the steeper temperature profile passing from operating condition A to B and C. Conditions B and C have temperature profiles which are almost parallel to each other, and this is visible both in the simulation results and in the experimental data. Figure 2 shows that the agreement between simulated and experimental data of solid temperature is very good at the cell midpoint, where the average model error is ≈1.4%. The error between calculated and simulated solid temperature is maximum at x = 9 cm (end-point), where the model error reaches ≈3.4% for condition C. Here, the shapes of the simulated curves deviate from the experimental ones, and this discrepancy is caused by

the fact that the model is adiabatic, while in the real system the temperature decreases due to heat dispersion at the cell borders.

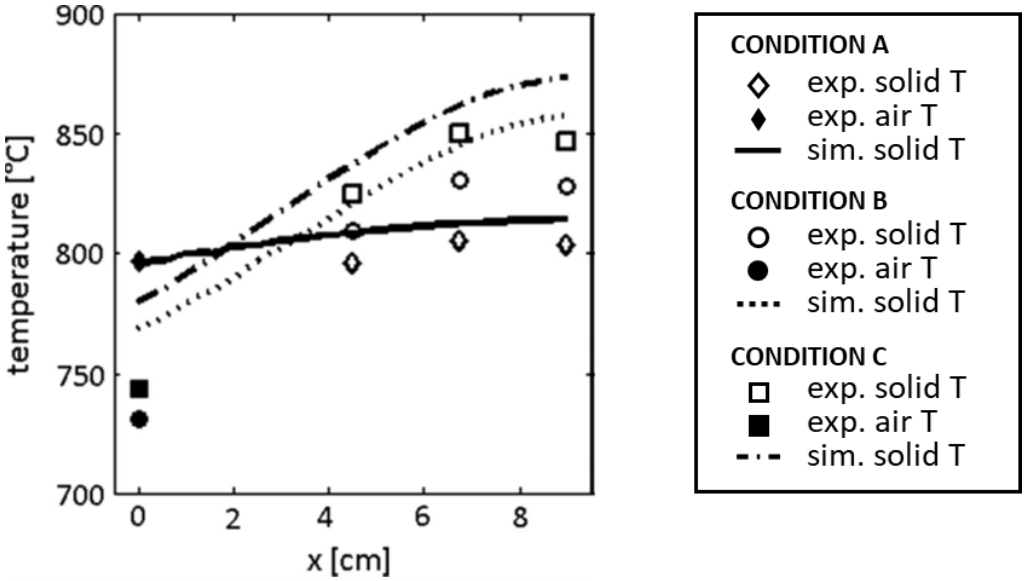

Figure 2. Temperature distribution along the cell coordinate.

Validation of the SOFC model under faulty conditions is presented and discussed in [9]. More specifically, the fault considered is a catalyst deactivation in the reformer, which leads to a reduced conversion of the methane steam reforming reaction.

Validation of the simulation model developed for the reformer was made by comparing simulation results to experimental data for the composition of the fuel at the exit of the reformer at various operating temperatures, as shown in Figure 3. Experimental values are evaluated on a dry basis (water is separated from the mixture before the analysis), and simulated results have been calculated in the same way. The agreement between simulated and experimental data is reasonably good (average error ≈10%), which confirms the validity of the hypothesis assumed to create the model. The agreement is particularly good for H_2 (error ≈2.5%), which is the most important chemical species for the SOFC stack simulation.

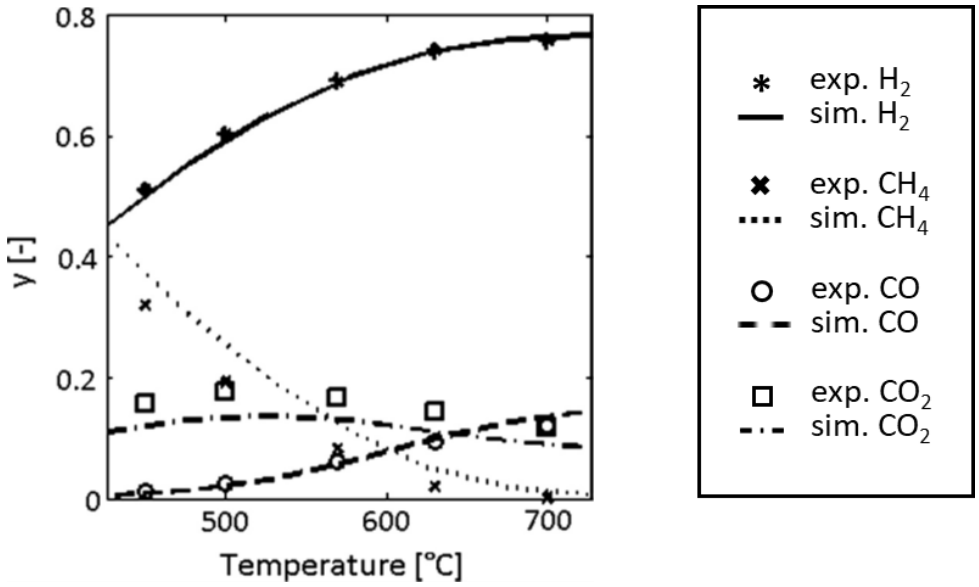

Figure 3. Reformer validation: molar fractions y at the outlet of the reformer (on dry basis).

The reliability verification of the other plant component models was carried out in the following works: [13] for the recuperator, [11] for the ejector and D1.5 [12] for the turbocharger devices. In [13] the recuperator is part of an externally fired micro-gas turbine system designed by Ansaldo Ricerche and the UNIGE. The model validation is based on experimental data collected running the system at different electric power loads. In [11] an ejector based anodic test rig developed at UNIGE is presented. Many tests were run on this rig using air or CO_2, at room temperature and at 150°C. The data collected during these tests were used to validate the ejector model based on pressure difference at the secondary Δp and recirculation factor F. In Figure 4 the validation using air flows both and at the primary and the secondary is shown. It can be seen that the model results are in good agreement with the experimental data.

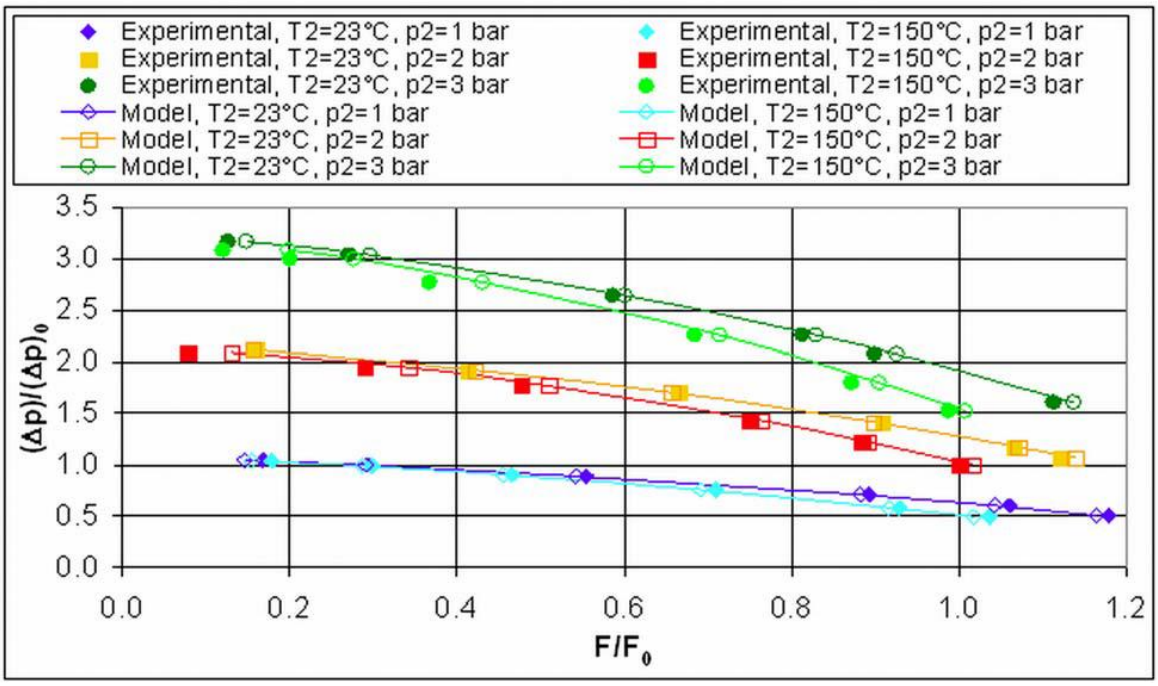

Figure 4: Ejector model steady-state validation

2.4 Results of simulations with the validated model

The results related to the steady-state analysis were obtained considering different operative conditions: fuel composition change (for obtaining a high fuel flexibility level), load change and variation of ambient temperature.

2.4.1 Fuel flexibility

The first set of simulations has been performed setting the model as a plant designed to operate with a 50% CH_4 -50% CO_2 (molar composition) bio-fuel and maintaining the fuel utilization factor (U_f) at 0.8 and the current density at 0.237 A/cm^2) [14]. Since fuel flexibility is an important feature of hybrid systems, many simulations have been carried out varying the bio-fuel composition from 50% CH_4 - 50% CO_2 to a CO_2 decrease up to 100% CH_4.

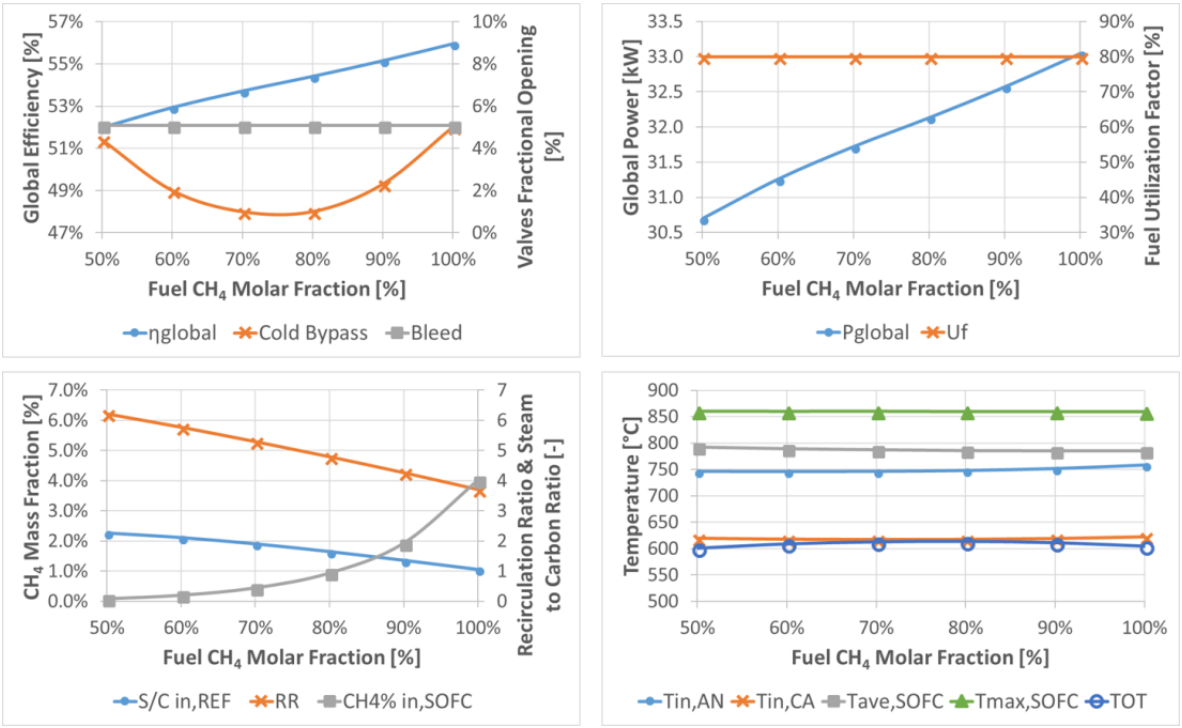

Figure 5: Performance of a turbocharged SOFC system designed to operate with a 50% CH_4 -50% CO_2 bio-fuel

Figure 5 shows that increasing the percentage of CH_4 the global power and efficiency of the system are higher, because of the fuel higher energy content. The SOFC voltage ranges from 0.715 V to 0.758 V with the same trend of the power. The bypass and bleed valve (see Figure 1 for the location) openings have been determined in order to comply with the SOFC operational constraints (SOFC maximum temperature equal to 860°C and difference between anode and cathode temperature lower than 250°C). Since the TOT is always lower than 650°C, a standard heat exchanger can be used as REC. The main issue of this system is that, for percentages of CH_4 higher than 70%, the S/C at the reformer inlet is too low [15] (due to a too low recirculation ratio, named RR in Figure 5, that is the ratio between the secondary and the primary flows of the ejector [11]). Switching from the 50% to the 100% case in CH_4 concentration, the RR is decreasing due to the pressure decrease at the ejector inlet (necessary to obtain the required fuel mass flow rate). Moreover, the mass fraction of CH_4 at the SOFC inlet is higher with higher percentages of CH_4 in the fuel, causing a more significant fuel cell internal reforming. Thus, the anodic ejector has been re-designed to correctly operate with a 100% CH_4 fuel and a new set of simulations have been performed (U_f always maintained at 0.8 and the current density at 0.237 A/cm^2).

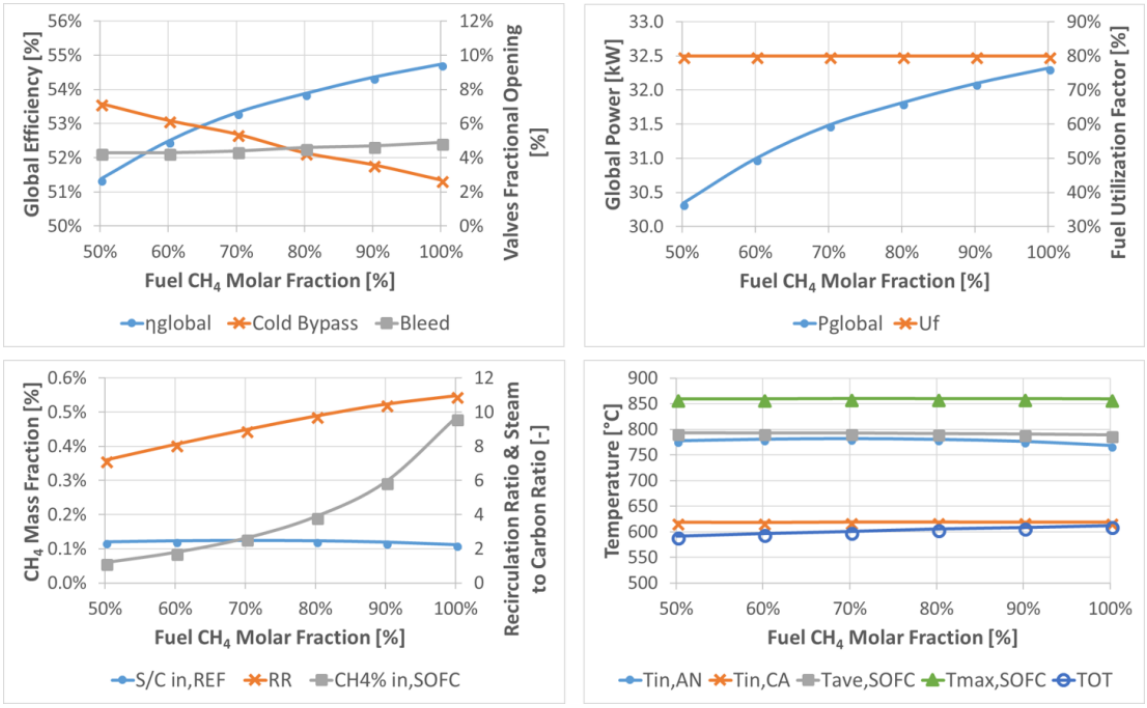

Figure 6: Performance of a turbocharged SOFC system designed to operate with a 100% CH_4 bio-fuel

Figure 6 shows that re-designing the ejector to have a significant RR increase, the S/C is higher than 1.8 (operational limit reported in [15]) for each considered bio-fuel composition. In addition, the mass fraction of CH_4 at the SOFC inlet is much lower than its values in the previous configuration. The RR trend of Figure 6 is the opposite in comparison of what reported in Figure 5, because in this case the primary nozzle is choked, differently from the subsonic behaviour considered for the Figure 5 case (see [11] for the momentum equation responsible of the RR trend). Like in the former set of simulations, the global power and efficiency of the system increase for higher percentages of CH_4. However, their values are slightly lower. The SOFC voltage ranges from 0.713 V to 0.741 V with the same trend of the power. All the SOFC operative limits are respected thanks to the regulation of the bypass and bleed valves and the TOT is kept under 650°C.

2.4.2 Part load conditions and ambient temperature effect: preliminary results

The model presented in chapter 2.2 was used to simulate the behaviour of the hybrid SOFC plant in different operating conditions. The results obtained from these simulations were used to carry out a design/off-design analysis considering the effect of different values of ambient temperature and current density (that is directly related to the SOFC power).

In the first set of simulations a control system acting only on the Wastegate Valve (WGV) was used (all the other valves were maintained fixed). The system design point was calculated at 15°C ambient temperature, with a fuel utilization factor U_f equal to 0.8. The related design

property values are the following: 30.56 kW net power produced and 51.7% global efficiency (interesting value considering bio-fuel and SOFC pressurized with a turbocharger). At design condition, it was necessary to consider a margin for the bypass valve (about 11.2% of the upstream mass flow bypassed through the valve) to have the necessary flexibility to compensate load and ambient temperature variations.

The current density could vary between 100% and 60% of its nominal value, equal to 0.237 A/cm^2. Ambient temperatures between -10°C and +40°C were considered. The WGV opening at different conditions was determined in order to comply with the many SOFC operational constraints, reported in Table 1.

Table 1: Operational constraints of the SOFC

Parameter	Unit	Value
Max temperature	°C	850÷860
Max AN-CA inlet T difference	°C	250
Max AN T difference	°C	250
Max CA T difference	°C	250

From these simulations it was possible to obtain the net global efficiency – power output map of the system, as shown in Figure 7. Lowering the current density, the power generated by the fuel cell decreases, thus the total net power of the plant drops. Since the internal losses are smaller, the fuel cell efficiency is higher at lower values of the current density (ohmic losses are directly proportional to it), in accordance with the typical fuel cells behaviour [7][16]. The global efficiency follows the same trend (Figure 7), because the electrical losses and the power consumed by the auxiliary systems decrease lowering the current density. At 60% current density and 15°C ambient temperature, the global efficiency reaches the value of 58.0%. When the ambient temperature is higher, the system is more efficient (Figure 7) thanks to the SOFC pressure increase reported in Figure 8. This effect is less distinct for lower loads.

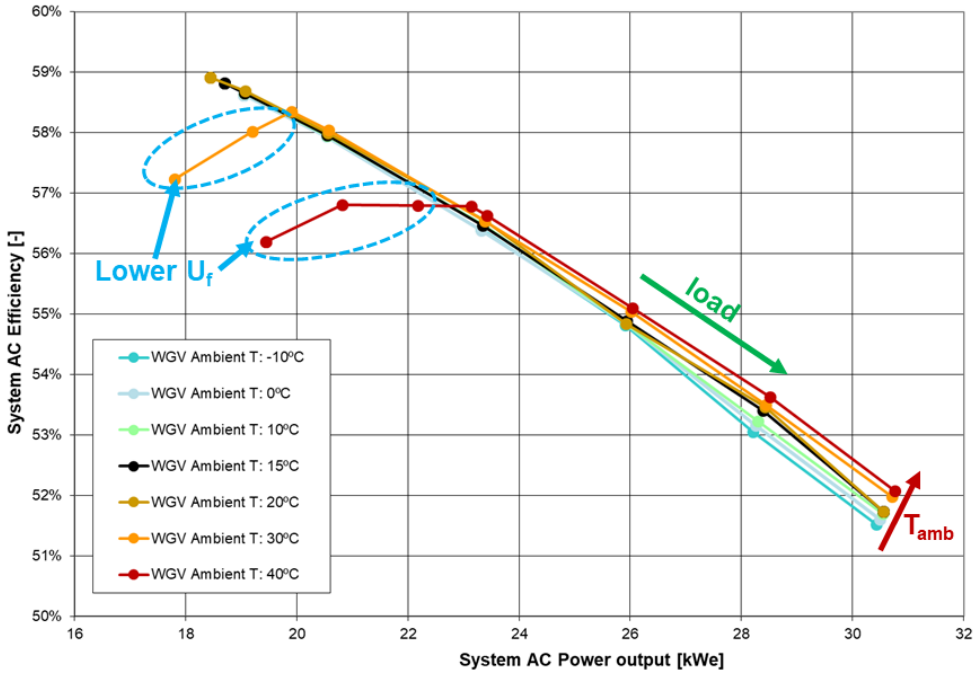

Figure 7: Global net efficiency of the system vs electrical power output at different ambient temperature conditions, with WGV control

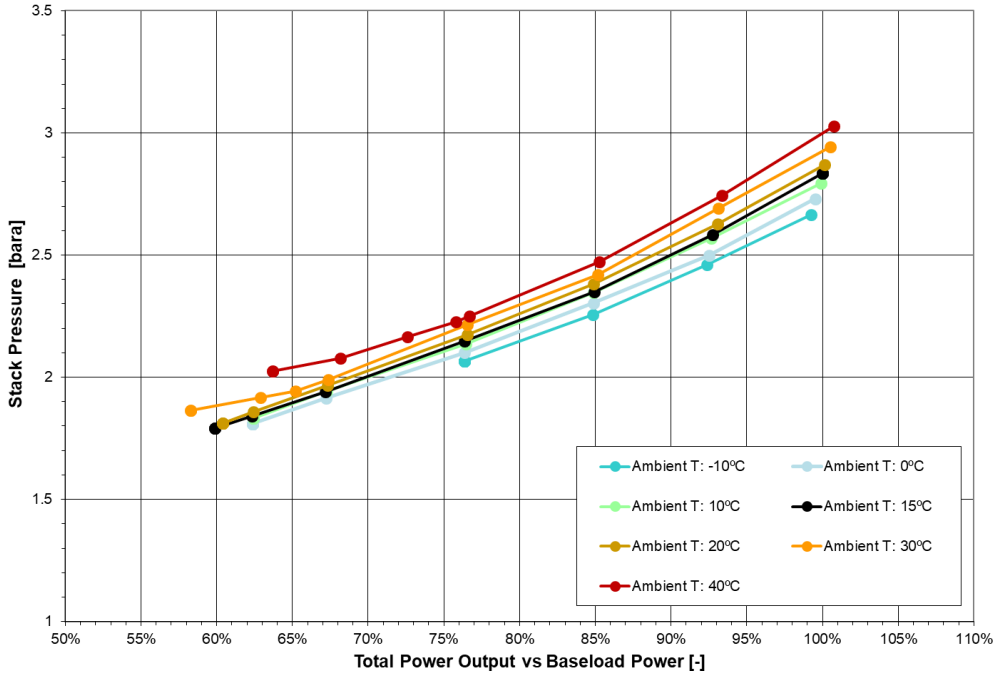

Figure 8: SOFC stack pressure vs power output percentage at different ambient temperature conditions, with WGV control strategy

It was observed that at low power loads, for high values of ambient temperatures (30°C and 40°C), it was not possible to comply the SOFC temperature constraints keeping U_f at the constant value of 0.8. To overcome this problem, U_f was reduced in these conditions, lowering the system global efficiency (Figure 7).

The main problem found using the WGV control in this set of simulations, is related to the high values of the turbine outlet temperature. One of the main goals of the Bio-HyPP Top-Economic layout is to have a lower investment cost compared to traditional gas turbine fuel cell hybrid systems. If the turbine outlet temperature is always kept under 650°C, it is possible to install a standard stainless-steel heat exchanger as air recuperator. Otherwise it is necessary to use a temperature resistant steel recuperator, whose cost is significantly higher. It is represented in Figure 9 that, for most of the considered operative conditions, the hot side temperature of the recuperator exceeds the 650°C limit.

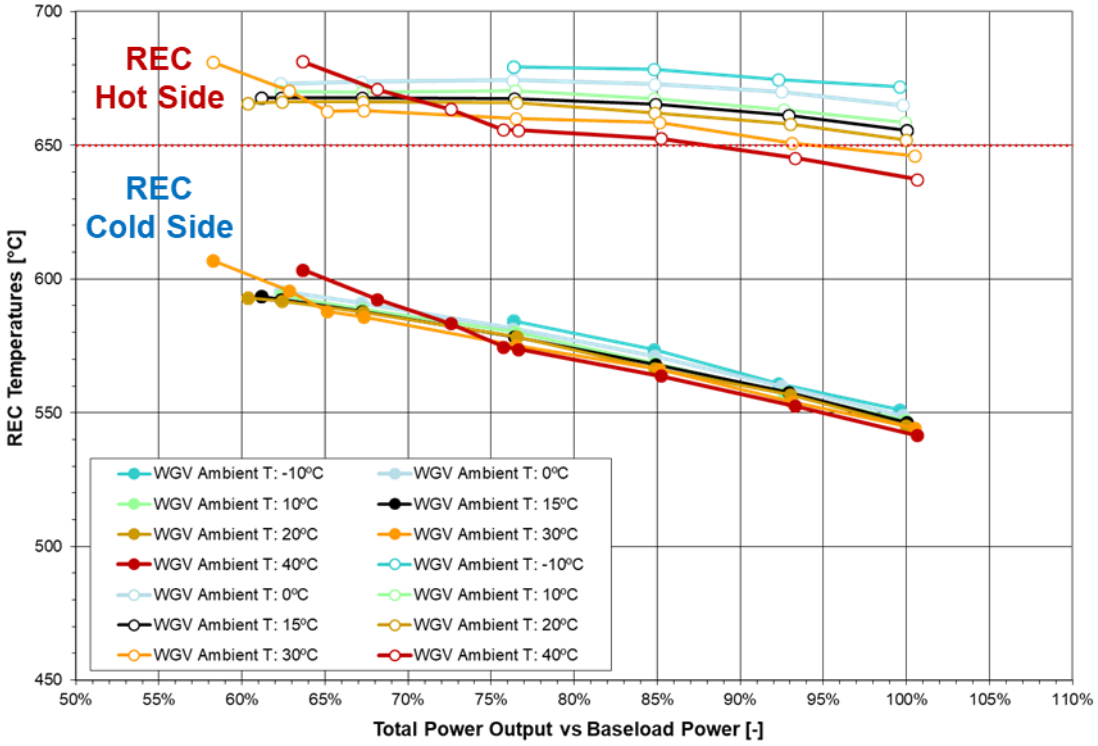

Figure 9: Recuperator temperatures vs power output percentage at different ambient temperature conditions, with WGV control strategy

Alternatives to the WGV control were investigated in order to overcome this problem. A first attempt was made using a Cold Bypass Valve (CBV) control to comply with the SOFC operational constraints. In this case the recuperator temperatures were always under the 650°C limit, as shown in Figure 10. However, this strategy has a negative impact on the system performance, as shown in Figure 11.

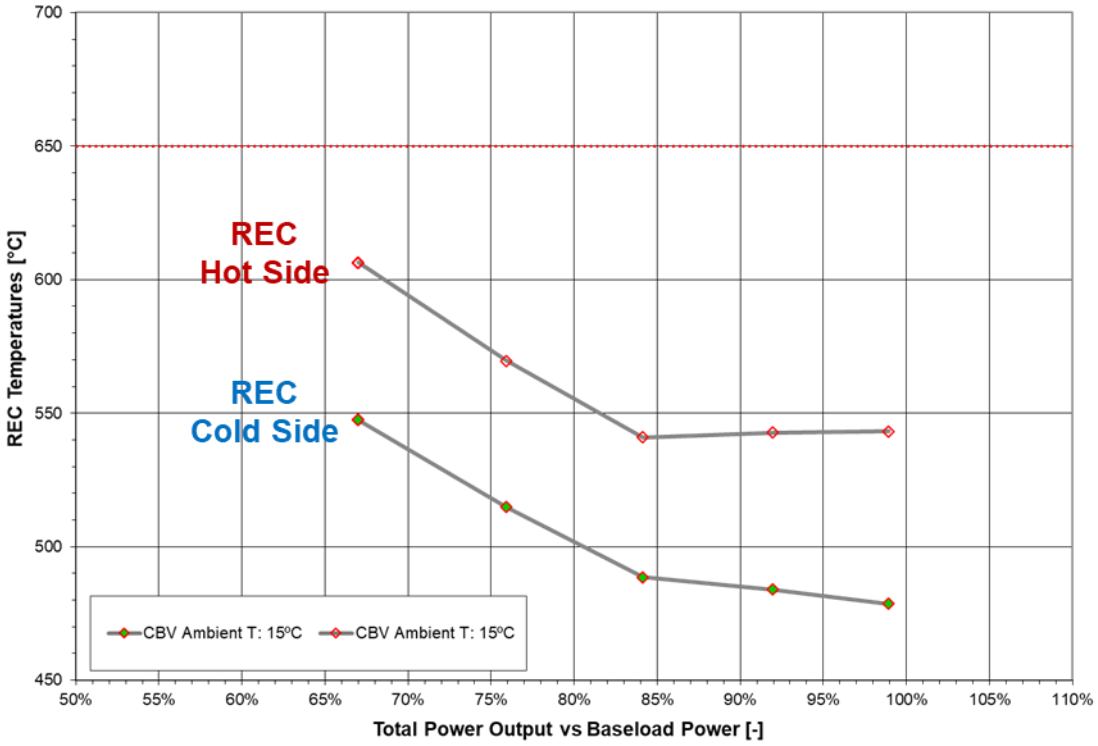

Figure 10: Recuperator temperatures vs power output percentage at design ambient temperature (15°C), with CBV control strategy

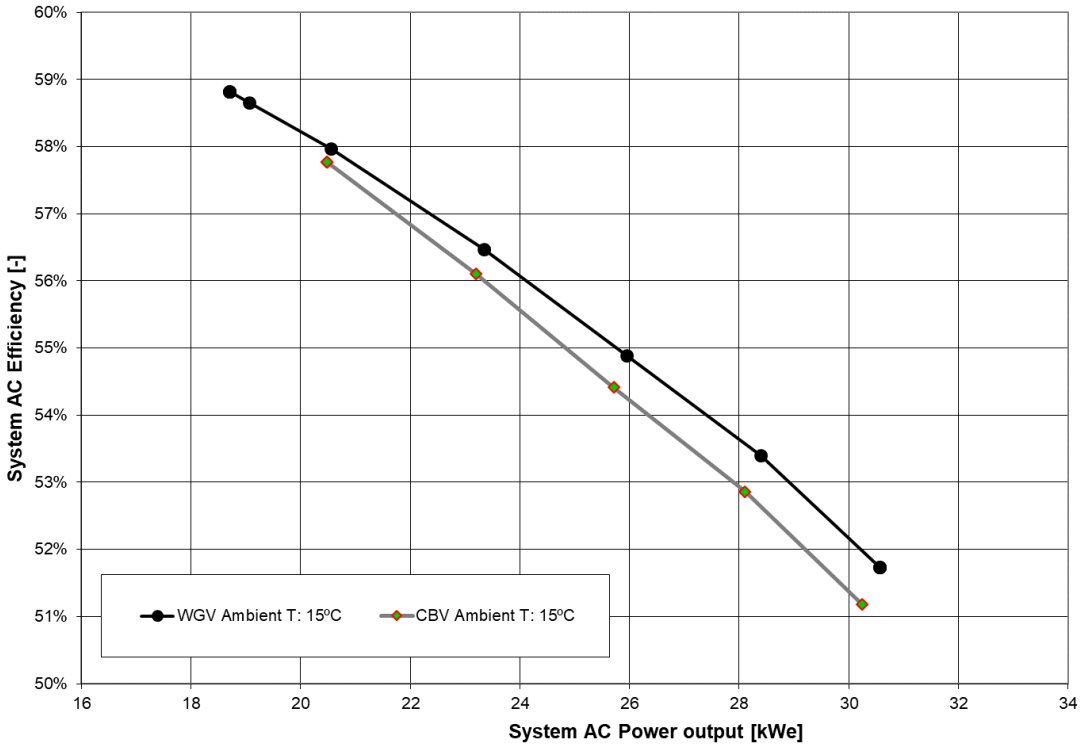

Figure 11: Global net efficiency of the system vs electrical power output at design ambient temperature (15°C), comparison between WGV and CBV control strategies

2.4.3 Part load conditions and ambient temperature effect: final results

To optimize the system both in terms of performance and of investment cost, a third control strategy was implemented, acting both on WGV and CBV to comply with all the SOFC constraints and to keep the turbine outlet temperature under 650°C.

Also in this case, the system design point was calculated at 15°C ambient temperature, with a fuel utilization factor U_f equal to 0.8. The related design property values are very close to the ones obtained with the WGV control: 30.54 kW net power produced (0.02 kW less) and 51.7% global efficiency (no significant variation). At design condition, it was necessary to consider a margin for both valves (upstream mass flow bypassed equal to 11.3% through the WGV and equal to 1% through the CBV) to have the necessary flexibility to compensate load and ambient temperature variations.

The current density could vary between 100% and 60% of its nominal value, equal to 0.237 A/cm^2. Ambient temperatures between 0°C and +30°C were considered.

Combining properly the openings of these two valves it was possible to obtain the net global efficiency – power output map reported in Figure 12.

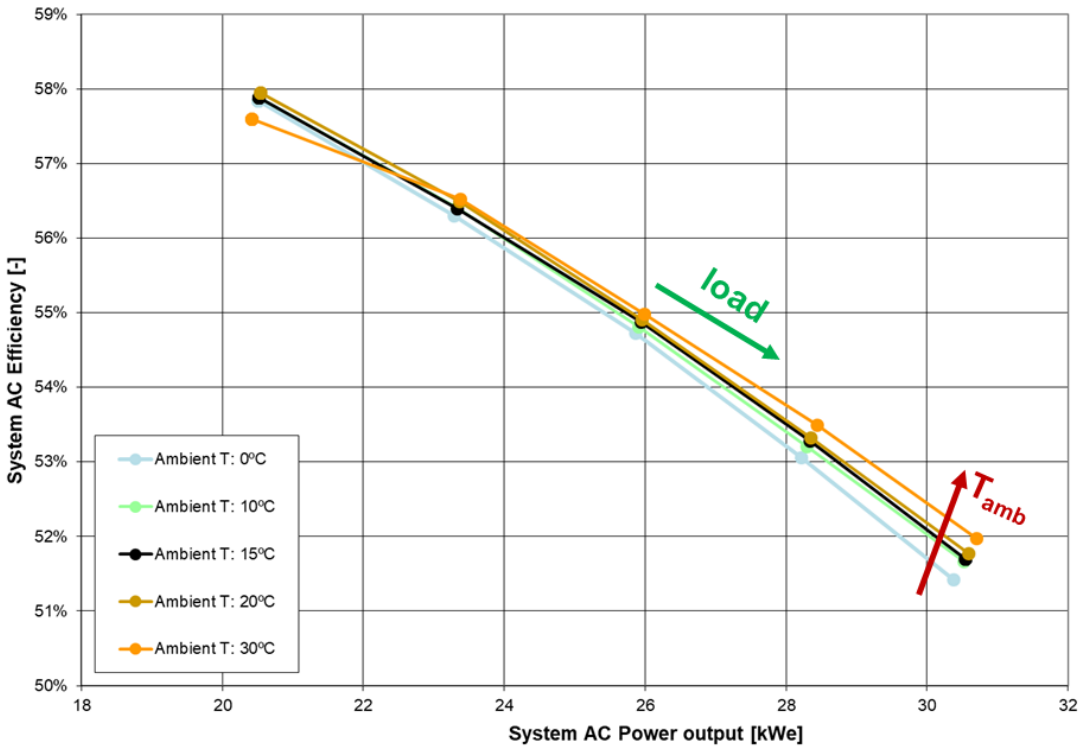

Figure 12: Global net efficiency of the system vs electrical power output at different ambient temperature conditions, with WGV+CBV control strategy

The trends are similar to those observed in Figure 7: the system efficiency increases lowering the power load and at higher ambient temperatures. However, it is not necessary to reduce the U_f value in any of the points of the 30°C curve to comply with the system constraints.

Figure 13 shows that it was always possible to keep the turbine outlet temperature under 650°C, thus a standard stainless-steel heat exchanger could be installed as air recuperator in this system. It is worth noticing that, with this control strategy, the recuperator temperatures are not significantly affected by the ambient temperature value.

When the current density is equal to 60% of the design value and the ambient temperature is 30°C, it is not possible to have a SOFC maximum temperature equal to 860°C while keeping the recuperator temperatures under 650°C. In fact, the SOFC maximum temperature is equal to 850°C in this condition. This temperature is within the SOFC temperature limits (Table 1), but leads to a slightly worse performance of the system (the leftmost point of the 30°C curve in Figure 12).

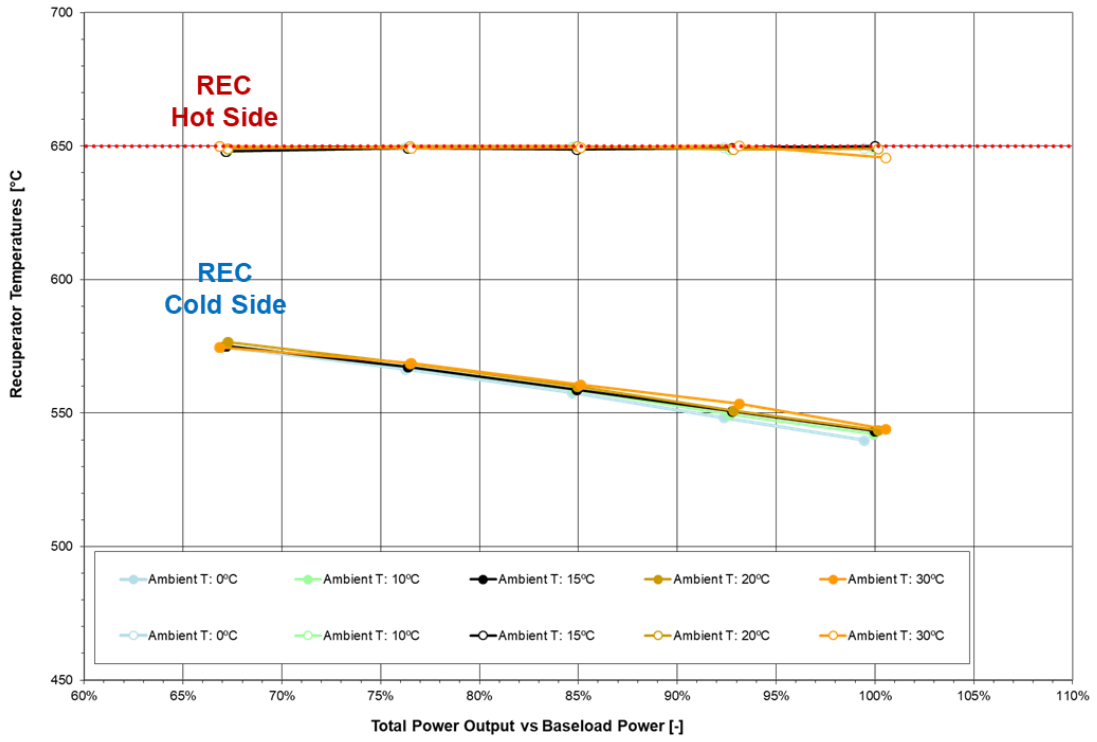

Figure 13: Recuperator temperatures vs power output percentage at different ambient temperature conditions, with WGV+CBV control strategy

2.5 Robust design of a turbocharged SOFC system (additional activity)

The results obtained in the WP1 moved the UNIGE team to perform a further additional activity (in comparison with the planned work of the Bio-HyPP project) [22].

The impact of the main operating parameters (fuel cell area, stack current density and recuperator surface) on the plant performance has been evaluated, considering uncertainties in the system and creating a response surface of the model to perform the study. Further on, a study of the operating costs of such plant was performed to evaluate its profitability in the Italian market scenario.

The uncertainties related to turbine and compressor efficiencies (η_t, η_c) and to the SOFC ohmic losses corrective coefficient (K_{ohm}) were considered. The uncertain parameters were described through a Gaussian probability density function (PDF), based on industrial data and authors' knowledge [23] (Table 2 - left). To create the response surfaces (RS) of the model described in Figure 14 the Central Composite Design Face Centred (CCF) method was used. The effect of three parameters (factors) on the performance and economic profitability of the hybrid system within the Italian market scenario was investigated. The factors are:

- Area of a single fuel cell (A_{cell})
- Exchange surface of the recuperator (S_{rec})
- Stack current density (J_{cell})

Table 2: Mean and Coefficient of Variance of the uncertain parameters (left) and factor levels considered for RS creation (right)

Variable	μ	COV
η_c [%]	72%	1%
η_t [%]	61%	1%
K_{ohm} [-]	0.48	3%

Factor	Name	Central Point	Low Level	High Level
A	A_{cell} [m^2]	0.01278	0.01150	0.01406
B	J_{cell} [A/cm^2]	0.237	0.213	0.261
C	S_{rec} [m^2]	8.03	7.23	8.83

Table 2 shows the values of the coefficients of variance (COV): they were evaluated as the ratio between the standard deviation and the mean of each single variable, providing improved understanding of how the PDF is spread. The response surfaces were created considering a 10% variation from the central point of the factors for low and high levels, to evaluate a hybrid system which would feature a different stack but without the necessity of changing the other components due to a huge variation of the SOFC stack features (Table 2 - right). A second-order RS meta model was built with Design Expert ® 11.0 with a three-level factorial design. A total of 75 runs with the simulation model described before were done, to perform a proper CCF, based on the following equation, performing each run 5 times (n° of repetitions) to consider the uncertainties in the system (1).

$$n^\circ\ of\ runs = n^\circ\ of\ repetitions\ (2^{n^\circ\ of\ factors} + 2 \cdot n^\circ\ of\ factors + 1) \quad (1)$$

The response surfaces were created for the net power and efficiency of the hybrid system and for the internal rate of return (IRR), considering an Italian market scenario and the hybrid system to operate at maximum load. The total initial investment was computed as a function of the costs of the main components of the hybrid system [24][24], while the annual cash flow considered for a 10-year life span of the system was computed as in (2).

$$CFN_j = C_{el} \cdot P_{NET} - C_f \cdot P_f - C_{maint} \quad (2)$$

The annual maintenance cost was calculated as the sum of 10% of the SOFC initial investment and 3% of the other components initial investment: this allows to take into consideration the substitution of the stack after 5 years, amortized along the time span set as end-of-life (EOL) of the plant. The main economic parameters used for this analysis are illustrated in the following table (

Table 3). The electrical price is favourable because of potential on-site self-consumption of the produced energy or renewable feed-in-tariff scenario.

Table 3: Economic parameters used for the analysis

Revenue	$C_{el} = 0.15\ €/kWh$
Operational Cost	$C_f = 0.27€/kg$ $C_{maint} = 10\%\ of\ SOFC + 3\%\ of\ other\ components$
Operating hours	$EOH = 8000\ h/yr$ $EOL = 10\ yrs.$

To identify the most suitable model (i.e. quadratic, linear, cubic) for the creation of the response surfaces of net power, efficiency and IRR, an ANOVA was performed and used to evaluate which single factor and combination of them were significant ($p_{value} < 10^{-5}$). The ANOVA suggested that a quadratic model was significant for representing the net power, resulting in a predicted R^2 of 0.9891 (i.e. maximum R^2 value would be 1 in case of perfect fitting of the RS with the model). This represents the degree to which the input variables explain the variation of the output/predicted variable, in good agreement with the adjusted R^2 of 0.9899, which gives the percentage of variation explained by only those independent variables that in reality affect the dependent variable. ANOVA suggested instead that a linear model would have been good enough to represent net efficiency and IRR. In

Table 4 the R^2 values of the three response surfaces are reported, as well as the deterministic nominal values of net power, net efficiency, IRR and their minimum and maximum values produced from the 75 runs performed under uncertainty, to build the RS.

Table 4: RS results

Response variable	Predicted R^2	Adjusted R^2	Nom. value	Min. Value	Max. Value
P_{net} [kW]	0.9891	0.9899	30.56	25.18	36.21
η_{net} [-]	0.8639	0.8716	51.75	48.97	53.79
IRR [-]	0.5530	0.5790	0.1736	0.1444	0.1963

It can be observed that the IRR presents a low R^2, suggesting that the model is not very representative of the real behaviour of this variable within the boundaries considered, related also to the strong impact of uncertainties on it. This result can be also highlighted from the RS representation presented in Figure 14(b), as the simulation points highlighted with red dots are more scattered than for the net efficiency R^2. Instead, the R^2 of net power and net efficiency is good and the RS obtained is then well representative of the plant performance.

The factors which have the strongest impact on net power, are cell area and current density, as it is directly related to them. The net efficiency is mainly influenced by current density and its increase for lower values of J_{cell} is due to the SOFC ohmic losses reduction. Net efficiency behaviour is however slightly different than net power behaviour, as it can be also observed from the R^2 value, as the efficiency also depends on the fuel mass flow which is computed from the model as a function of current density and cell area.

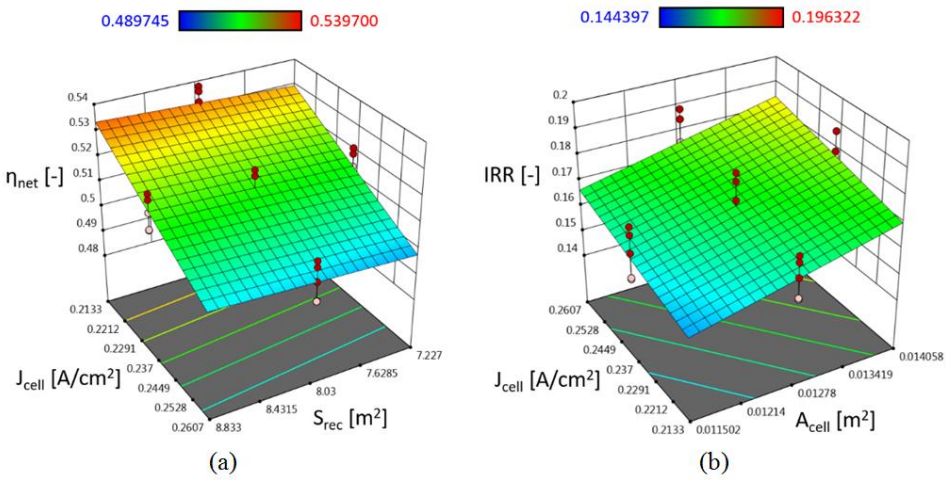

Figure 14: Response surfaces of (a) net efficiency as a function of J_{cell} and S_{rec} (A_{cell} = 0.01278 m²) and (b) IRR as a function of J_{cell} and A_{cell} (S_{rec} = 8.03 m²)

The factors which have the strongest impact on IRR are the current density and the cell area, as they both impact directly the net power and so the revenues, despite a higher cost of the SOFC stack, while the recuperator surface has a particularly low impact on the IRR. Within the scenario considered in this work, it appears to be more important to sell as much energy as possible to increase the profitability of the plant. In a scenario with higher natural gas price and lower electricity value, the conclusions could differ.

3 Thermodynamic Performance Modelling of top-performance layout [author: DLR: Thomas Krummrein, Marius Tomberg]

3.1 System layout and model description

The layout of the SOFC/MGT hybrid power plant concept at DLR can be seen in Figure 15. The layout has been the basis for deriving the two separate test rigs (real MGT with emulated SOFC and real SOFC with emulated MGT).

The simulation tool for the SOFC/MGT hybrid power plant has been described in detail in [27]. This chapter focusses on the validation of these models with measurement data from the DLR test rigs.

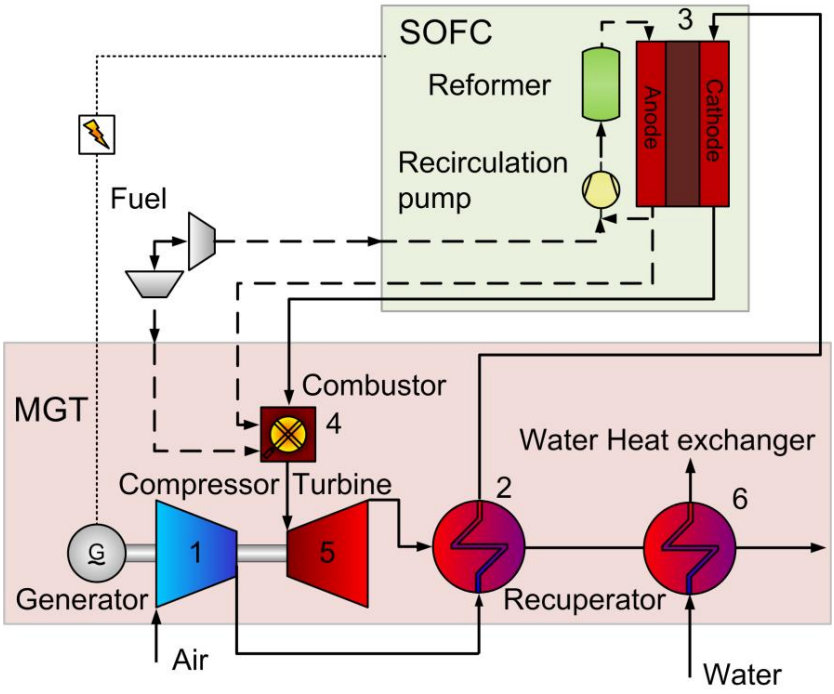

Figure 15: Simplified block diagram of the SOFC/MGT hybrid power plant concept [27]

3.2 SOFC subsystem model validation

3.2.1 Model description and parametrization

The SOFC test rig at DLR contains a real SOFC and components that emulate the MGT. The SOFC subsystem, consisting of the SOFC module, the recirculation system and the reformer, is placed inside a pressure vessel. This pressure vessel and the contained components are tested in the SOFC test rig. Therefore, the data gained from experiments on the SOFC test rig will be used to validate the model for the SOFC system.

Figure 16 shows the components of the SOFC subsystem model as well as the quantities used in the validation.

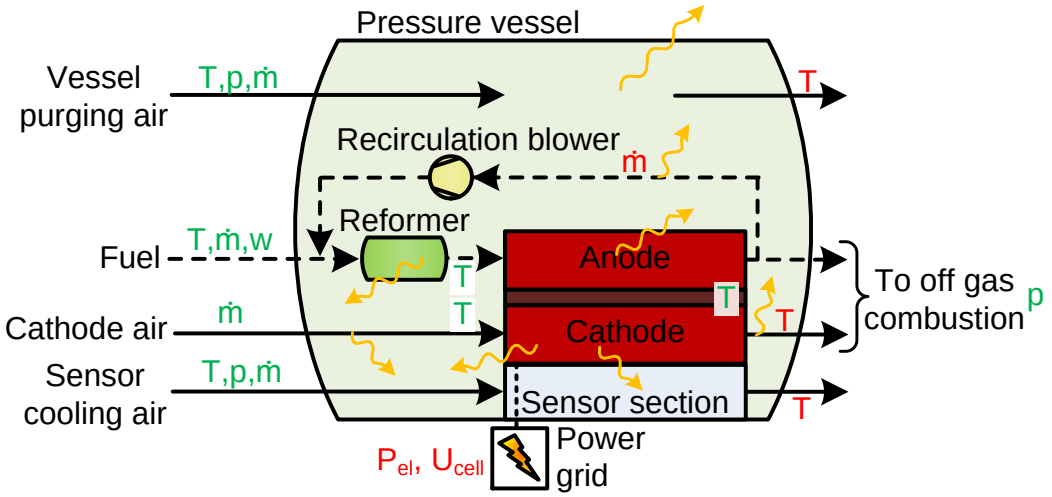

Figure 16: SOFC Subsystem used for validation with heat losses (orange arrows), specified quantities (green) and validated quantities (red).

The main component model is the SOFC model that merges all SOFC modules into a 0D model of anode and cathode side. Deliverable 1.2 [27] describes the model in more detail. The electrochemical model and parametrization is equivalent to the model described by Steilen [29]. It computes the average SOFC cell voltage from the Nernst voltage at the SOFC module outlet using a temperature dependent area specific resistance (ASR). The ASR is based on experimental data of 10 layer stacks [29]. As mentioned in deliverable 1.2 [27], the outlet temperatures of both the anode and the cathode sides are assumed to be identical and are equal to a specified stack core temperature. Pressure losses are considered for the cathode side and the anode side respectively. In addition, both sides calculate a heat loss to the inside of the pressure vessel. Furthermore, a heat loss from the cathode side to the sensor section is assumed that is flowed through with cooling air. This heat loss is proportional to the difference of reference temperatures of the cathode side and the sensor section, where the reference temperature is the mean value of inlet and outlet temperature.

For the reformer chemical equilibrium at the outlet is assumed [27]. The recirculation blower is modelled as a compressor, which compensates the pressure losses of the components in the recirculation loop. The efficiency of the compression is computed with a simple linear correlation in dependency of the volume flow, which is based on manufacturer data [29].

The piping is represented by a pressure and a heat loss between each component.

3.2.2 Model validation

The SOFC subsystem is validated using data of five static points. Figure 16 shows the quantities used in the validation: The quantities marked red are specified in the validation simulations with measurement data. Green quantities are used for validation of the simulation results with measurement data. However, there are certain limitations in the validation process: It is not possible to validate pressure losses because pressure measurements were performed with absolute pressure sensors. The measurement uncertainty of these sensors is larger than the pressure difference (see also section 3.3.2). Furthermore, there is a quite large distance between the pressure vessel outlets of the SOFC off-gases to the next temperature measurement. Because these pipes are influenced heavily by unknown heat losses, the real temperature at the pressure vessel outlets cannot be determined and, therefore, not be validated.

The temperature measurement for the cathode off-gas between the SOFC module and the pressure vessel outlet is assumed to be the vessel outlet temperature, ignoring temperature losses of the vessel feed-through and some piping. Finally, the recirculation mass flow is a validation quantity, but it is not directly measured. Instead, it is estimated using a method of deliverable D2.5 [30] with high uncertainties.

Table 5 shows the measurement data of the five operation points (OP) used for validation, which are specified in the SOFC subsystem model simulations. The points cover different fuels as well as variations in the system pressure and electrical output. Table 6 shows the values of the measured versus the simulated values of the electrical power, the current, the voltage, the recirculation mass flow and some temperatures.

Table 5: SOFC subsystem validation points – specified values in validation simulation

	OP1	OP2	OP3	OP4	OP5
Fuel composition [m-% NG/H_2/CO_2]	86/14/0	0/100/0	55/45/0	36/10/54	0/100/0
Fuel flow [g/s]	0.552	0.506	0.390	0.984	0.216
Fuel inlet temperature [K]	302	302	298	302	301
Cathode air flow [g/s]	27.8	46.9	38.1	22.6	28.8
System pressure [bar]	2.00	3.00	2.00	1.80	1.08
Mean SOFC temperature (normalized)	0.985	0.987	0.981	0.980	0.980
SOFC anode inlet temp. [K]	923	923	923	923	923
SOFC cathode inlet temp. [K]	980	907	989	968	972
Purging air inl. temperature [K]	316	431	426	433	430
Purging air mass flow [g/s]	9.3	15.7	12.7	8.1	9.6
Sensor section air temp. in [K]	302	298	300	296	298
Sensor section air flow [g/s]	28.4	35.7	32.2	31.8	31.5

Table 6: SOFC subsystem validation points – measured values, simulated values (italic) and deviation

	OP1	OP2	OP3	OP4	OP5
SOFC el. Power (normalized)	0.78 *0.77* -1.87%	1.00 *1.12* 11.50%	0.72 *0.71* -0.97%	0.68 *0.69* 1.52%	0.54 *0.56* 3.38%
SOFC cell voltage (difference to minimum value) [V]	0.06 *0.04* -1.82%	0.06 *0.07* 1.26%	0.07 *0.06* -2.10%	0.05 *0.05* -0.19%	0.10 *0.06* -4.41%
SOFC current (normalized)	0.78 *0.78* -0.05%	1.00 *1.10* 10.11%	0.71 *0.72* 1.16%	0.69 *0.70* 1.71%	0.51 *0.56* 8.15%
Recirculation mass flow [g/s]	17.8 *19.6* 10.4%	9.5 *8.7* -7.87%	12.0 *11.1* -7.90%	16.9 *18.2* 7.68%	8.8 *4.30* -51.3%
Temp. difference SOFC core – cathode off gas outlet [K]	53.7 *51.0* -0.25%	56.8 *28.3* -2.71%	44.9 *34.0* -1.03%	58.5 *57.1* -0.14%	48.0 *44.2* -0.36%
Temp. difference outlet – inlet of pressure vessel [K]	161.4 *201.3* 8.35%	79.1 *60.2* -3.70%	68.6 *70.3* 0.34%	75.1 *81.3* 1.22%	51.9 *78.4* 5.49%
Temp. difference outlet – inlet of sensor section [K]	55.1 *59.2* 0.97%	47.2 *45.5* -0.49%	49.9 *52.8* 0.82%	55.0 *53.0* -0.57%	55.3 *53.5* -0.50%

The most important validation quantities are the electric power of the SOFC system and the SOFC cell voltage since these quantities characterize the main component. It can be seen that the quite simple 0D modelling approach, which is parameterized with experiments using single stacks, results in good agreement with the experimental data for most cases. An exception is OP2 where the simulated SOFC electrical power is about 11.5 % above the measured power. This deviation is probably caused by a larger temperature gradient in the fuel cells: The difference between the mean SOFC temperature and the cathode inlet temperature is about 200 K for OP2 but only about 130 K for the other validation points. Because of this larger temperature gradient, the ASR varies too much over the fuel cells, which is not considered by the 0D model. To investigate this behavior in more detail, the spatial discretized cell model presented in [31] is extended to a complete module model by the DLR institute of engineering thermodynamics (DLR-TT) is currently developing.

However, besides OP2, the validation shows in general a good agreement of the model with the measurement data with deviations of only a few percent. The only quantity with larger deviation is the recirculation mass flow. However, as mentioned, the validation values are not measured but calculated and therefore cannot be compared directly.

3.3 MGT subsystem validation

The MGT test rig at DLR emulates the SOFC subsystem components while using real components of the MGT. Since the piping of the test rig differs significantly from the expected piping of the real hybrid power plant, a validation needs to be carried out individually for each component. The main components of the MGT considered are the compressor, the turbine, the recuperator and the combustion system.

Measurement data is available for five steady state points with air mass flows between about 27 g/s and 48 g/s. Furthermore, measurement data of a turbomachinery map measurement is available, which is steady state with respect to the air mass flow, but not with respect to all system temperatures. This data can be used to validate pressure losses and turbomachinery maps, but no heat losses or heat transfer related phenomena.

3.3.1 Turbomachinery

Compressor and turbine determine the pressure ratio and the air flow of the hybrid power plant system. In the Bio-HyPP project, the turbomachinery of the MTT EnerTwin are used which have a shaft speed up to 240 krpm. In the simulation model, turbomachinery maps characterize compressor and turbine. Each of them is described by a flow map, which represents the relationship between the reduced mass flow, the reduced shaft speed and the pressure ratio, and an efficiency map, which represents the relationship between the reduced mass flow or pressure ratio, reduced shaft speed and isentropic efficiency (eg. [32]).

These maps can be determined at the DLR MGT test rig by varying the shaft speed for specific bleed air valve or throttle valve positions. To interpolate the measurement and to extrapolate in certain limits, the data is fitted with 2D-polynomials using reduced quantities. These polynomials are used to create the maps in the representation described above. The degrees of both dimensions of the polynomial are chosen quite large to achieve a close fit to the measurement data. However, such large degree polynomials tend to undulations in the interpolation range and to nonphysical behavior and very steep gradients just outside the interpolation range. Therefore, additional conditions to some derivatives in a specified computation range are set to achieve both, a good fit of the measurement data as well as physical inter- and extrapolation. Such conditions can be divided into two groups: Some of them are general limitations for physical meaningful turbomachinery maps, e.g. the sign of a specific derivation. Some other conditions are set according to the values of a derivation in the interpolation range to prevent too strong changes in the extrapolation range. Such conditions are, somehow, arbitrary. However, since extrapolations with purely mathematical models are generally only of limited reliability, this can be used to incorporate experience about the general appearance of turbomaps into the extrapolation range.

3.3.1.1 Compressor

The flow map of the compressor is created using a 2D-polynomial of the pressure ratio Π in dependency of the flow coefficient Φ and the reduced shaft speed N_p. The isentropic efficiency is created using a further 2D-polynomial in dependency of the flow coefficient and the reduced shaft speed. Table 7 lists the properties of these polynomials.

Table 7: Properties of polynomials for compressor map inter- and extrapolation

Map	Degrees of 2D polynomial	Derivation conditions
Flow map $\Pi(\Phi, N_p)$	$\Phi: 6$ $N_p: 6$	$\frac{\partial^2 \Pi}{\partial \Phi^2} < 0$ $0 < \frac{\partial \Pi}{\partial N_p} < 4 \cdot 10^{-4} \frac{\sqrt{K}}{rpm}$
Efficiency map $\eta_{is}(\Phi, N_p)$	$\Phi: 9$ $N_p: 9$	$-95 < \frac{\partial^2 \eta_{is}}{\partial \Phi^2} < 0$ $-2 \cdot 10^{-8} \frac{K}{rpm^2} < \frac{\partial^2 \eta_{is}}{\partial N_p^2} < 0$ (only in extrapolation range)

The polynomials are able to fit the measurement data very well. The coefficient of determination R^2 for the flow map is larger than 0.99, for the efficiency map about 0.93. Figure 17 shows the resulting compressor map.

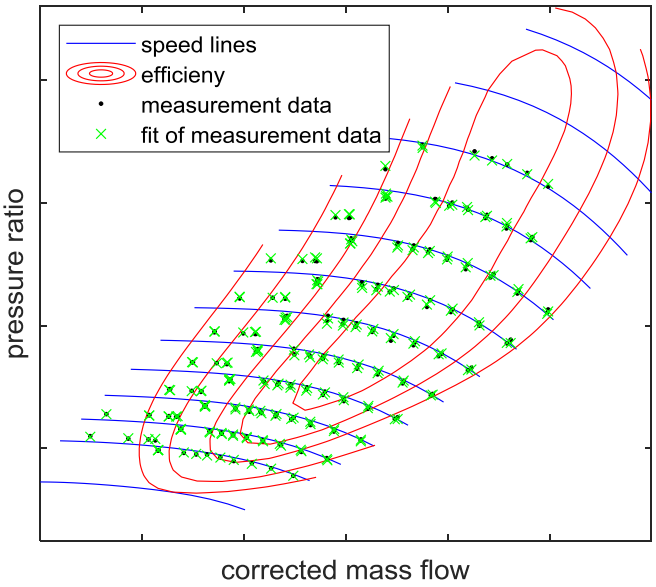

Figure 17: Compressor map

3.3.1.2 Turbine

The measurement of the turbine maps is much more difficult than the measurement of the compressor map: First, the temperatures are much higher and therefore the impact of heat losses can be quite strong, such that the measurement data indicates unrealistic large efficiencies. Second, the measurement of the turbine inlet temperature is quite difficult, because it is the highest temperature in the system. Furthermore, because the measurement of the turbine inlet temperature is just behind the combustion system, the gas temperature profile is not constant. In addition, only 2 of 5 turbine inlet temperature thermocouples were available for the measurement (as they broke sequentially while running experiments). Therefore, the measured data of the turbine inlet temperature are unreliable, especially since the measured values contain inconsistencies to other measurement data.

Since no turbine inlet temperature is available, the efficiency of the turbine cannot be determined. Instead, the turbine efficiency is described by an assumed function. Using an approach of Payri [33], a polynomial of degree 2 in dependency of the blade-to-jet-velocity ratio V_r is used. The parameters of the polynomial are chosen quite arbitrary with respect to existing turbine maps and qualitative consideration of the measurement data:

$$\eta_{is,turb} = 0.85 - 5 \cdot (V_r - 0.7)^2 \quad (3)$$

For most of the measurement points, this leads to a difference of the turbine inlet temperature of +5 K to -15 K to the original measurement data. Therefore, the impact of this adaption is not too large, but decisive for meaningful description of the turbine.

Using this relation to calculate the turbine inlet temperature, the flow correlation can be fitted using a 2D polynomial. According to an approach of Payri [33], the effective nozzle cross section A_{eff} is fitted in dependency of the blade-to-jet-velocity and the reduced shaft speed. The effective nozzle cross section is the cross section of an ideal nozzle with the same pressure ratio and mas flow as the turbine. Table 8 summarizes the used fit polynomials.

Table 8: Properties of polynomials for turbine map inter- and extrapolation

Map	Degrees of 2D polynomial	Derivation conditions
Flow map $A_{eff}(V_r, N_p)$	V_r 3 N_p : 3	$\frac{\partial A_{eff}}{\partial V_r} < 0$ $\frac{\partial A_{eff}}{\partial N_p} > 0$ $A_{eff} > 2 \cdot 10^{-5} m^2$
Efficiency map $\eta_{is}(V_r, N_p)$	V_r : 2 N_p : 0	$\eta_{is} = 0.85 - 5 \cdot (V_r - 0.7)^2$

The flow polynomial fits the measurement data very well with a coefficient of determination R^2 larger than 0.99. Figure 18 shows the resulting turbine map. It shows that the deviation of the flow is very small to the measurement data. The turbine is operated in the non-choking area.

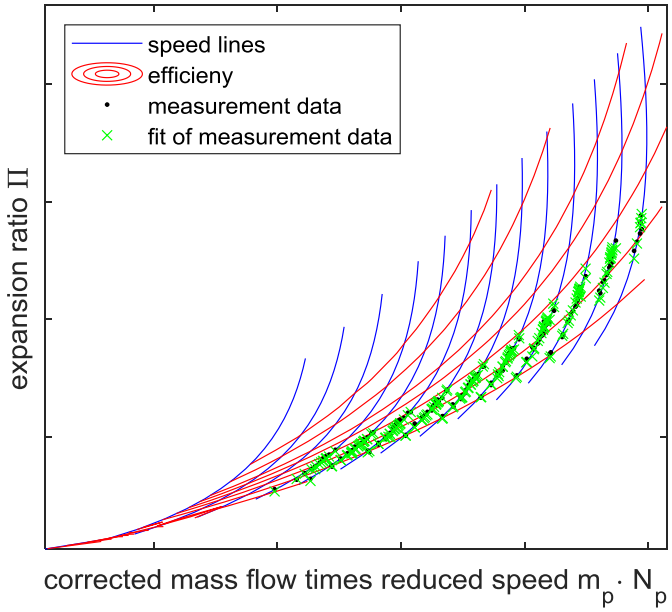

Figure 18: Turbine map

3.3.2 Recuperator

Figure 19 shows the pressure difference according to the measurements of the recuperator air side inlet and outlet. It can be seen that this pressure difference, which corresponds to the pressure loss, is always below 2000 Pa, yet it seems highly random and no correlation can be seen. The reason behind that is that measurement data is only available for absolute pressures with a measurement inaccuracy of 1000 Pa. Since all measured pressure differences are between -2000 Pa and 2000 Pa (double measurement inaccuracy), the data cannot show a correlation, but represents measurement inaccuracies. Therefore, it has been shown that the pressure losses are smaller than 2000 Pa for sure.

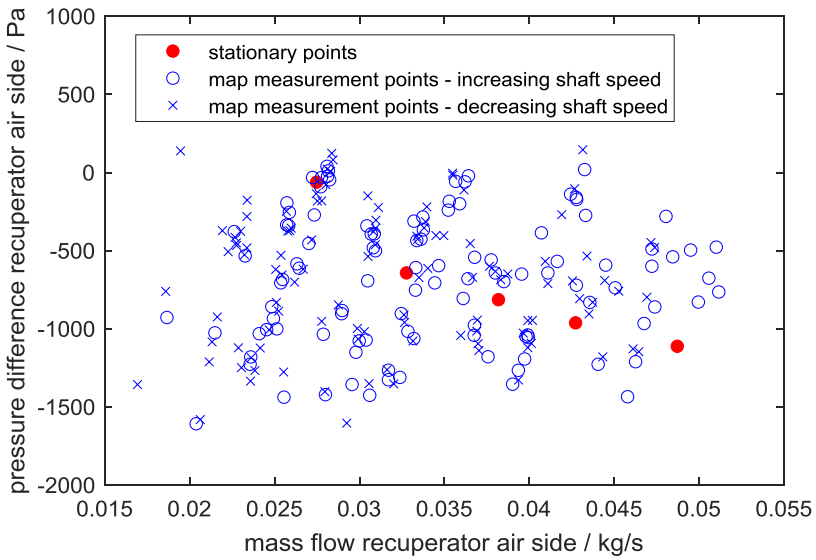

Figure 19: Pressure losses of recuperator air side

Figure 20 shows the efficiency and the heat losses over the air mass flow, calculated from the steady state measurement data. For the efficiency, the quotient of enthalpy difference and maximum possible enthalpy difference is calculated for both sides individually. The efficiency is the maximum of both values [34]:

$$\eta_{Recu} = \max\left(\frac{\int_{T_{in,1}}^{T_{out,1}} c_{p,1}(T)dT}{\int_{T_{in,1}}^{T_{in,2}} c_{p,1}(T)dT}, \frac{\int_{T_{in,2}}^{T_{out,2}} c_{p,2}(T)dT}{\int_{T_{in,2}}^{T_{in,1}} c_{p,2}(T)dT}\right) \quad (4)$$

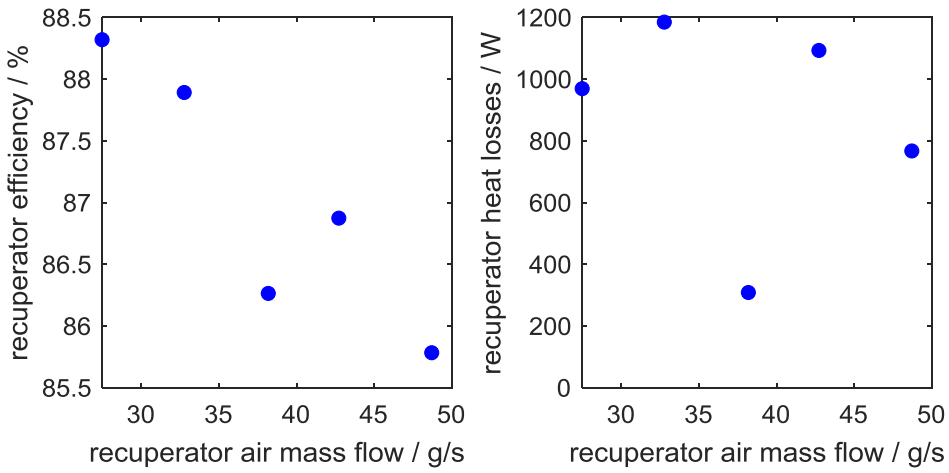

Figure 20: Efficiency and heat losses of recuperator

The third measurement point with an air mass flow of about 38 g/s seems to have a different behavior than the other steady state points. This is, because accidentally the vessel emulator heater was out of order and, therefore, the air inlet temperature of the recuperator for this state was significantly lower: It is approximately 92°C while about 270°C to 290°C for the other steady state points. In contrast, the exhaust inlet temperature is approximately constant for all steady state points (725°C to 755°C). This results in three conclusions of Figure 20:

1. First, the air inlet temperature has a significant impact on the heat losses, which seems to be stronger than the impact of the much higher temperature of the exhaust gas inlet. This may be explained with the design of the recuperator's insulation: the most heat loss seems to be at the exhaust outlet.

2. Second, the heat losses of the recuperator can be quite large and vary significantly. This is not only true for the absolute heat losses but also the heat losses compared to the exchanged heat between the exhaust gas and the air: The losses vary from about 1.3% (steady state with lower air inlet temperature) up to about 8.5% (steady states with low air mass flow) of the exchanged heat. Since for the real hybrid power plant the recuperator inlet temperature will also not be constant, this is an important factor.

3. Third, the impact of the air inlet temperature on the efficiency, which can be explained using the definition formula of recuperator efficiency (4)): Because of the design of the recuperator (the air path is located inside the exhaust gas side), heat losses are expected only at the exhaust gas side. Such heat losses increase the enthalpy difference at the exhaust gas side, without changing the maximum possible enthalpy difference. Therefore, the recuperator efficiency increases without increasing the actually exchanged heat. This explains why the point with the least heat losses seems to have the lowest efficiency. Consequently, the efficiency equation (4) may not be suited to describe a recuperator with large heat losses. Further investigations indicate that a model of an ideal recuperator without heat losses and an additional heat loss

only at the exhaust gas outlet could reproduce the experimental data. However, there is too little measurement data to validate such an assumption at current state.

Because of the heat loss uncertainty, it seems currently to be the best assumption to use a constant recuperator efficiency of about 87% in the model while being aware that the actual recuperation efficiency could deviate by a few percentage points. As soon as further measurement data will be available, the results will be validated further.

3.3.3 Combustion system

Since the 0D simulation model assumes complete combustion, heat and pressure losses of the combustion system can be validated with this model.

The measurement of heat losses is hard to do on the MGT test rig and a few of the turbine inlet temperature thermocouples have been broken during the experiments (as described in chapter 3.3.1.2). Therefore, the validation focus has been laid towards the pressure drop in the combustion chamber:

As described in deliverable D1.2 [27], pressure losses are described using an approach similar to Darcy-Weisbach. Using this approach, a pressure loss coefficient of $2.73 \cdot 10^6 m^{-4}$ can be determined. Figure 21 shows the measured pressure losses of the combustion system as well as the pressure loss simulated by the model. It can be seen, that there is still a small unexplained systematic deviation. However, the deviation is below the measurement inaccuracy (2000 Pa).

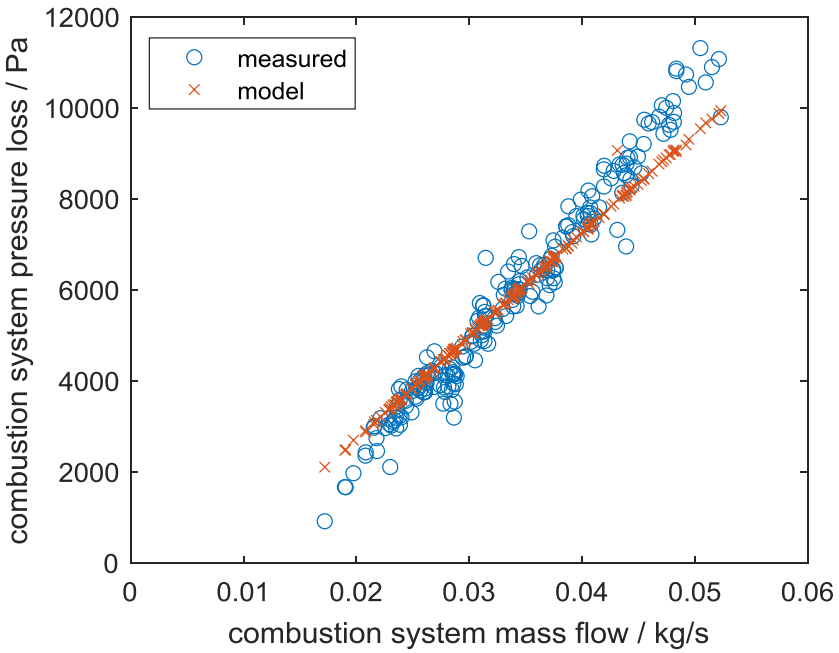

Figure 21: Pressure losses of combustion system

4 Dynamic Modelling and Control System [author: UNIGE: Mario Ferrari, Luca Mantelli]

The steady-state simulations performed in chapter 2.4 are very useful to analyse the system behaviour with different fuel compositions, power loads and ambient temperatures. However, from these data it was not possible to study the dynamic behaviour of the system. This information is crucial to find a proper control strategy able to comply with the system operative constraints during transient operations (e.g. power load changes). For this reason, a dynamic model of the system was developed.

4.1 Model description

A dynamic model of the Bio-HyPP Economic Layout was developed in Matlab®-Simulink® to study the behaviour of the system during transients and to develop a control system. As for the model presented in chapter 2.2, a 30 kW size system was considered. The component models are part of TRANSEO, an original tool developed by UNIGE for the transient and dynamic simulations of energy systems [17]. The dynamic behaviour of an energy system is mainly related to the mass and energy balances; momentum balance related effects, such as pressure wave propagation, are normally neglected. Nevertheless, TRANSEO is provided with dynamic models of a few components (i.e.: pipe and ejector components), which can be employed for the full dynamic analysis of their behaviour [18]. Unfortunately, this approach is very time-consuming and it is seldom worth extending the full dynamic analysis to the whole cycle. Most cycles can be effectively simulated on a transient basis, which already provides sufficient accuracy, as demonstrated by the validation results.

Within the transient models, at least two approaches are possible: the "mass continuity" approach [19] and the "interconnecting volume" approach [20][21]. The "mass continuity" approach forces the mass flows through each component to be consistent with the connected devices, that is considering steady-state mass flows at each time step: in turn, this involves neglecting the mass storage within and between components. The "interconnecting volume" approach allows mass flow mismatch to happen between subsequent components, by introducing plena to compensate for the mismatch, as each plenum changes its state (pressure, temperature) correspondingly.

More details about the TRANSEO tool can be found in [17].

The model is organized in two main blocks: TC, including turbocharger, recuperator, valves (Cold Bypass, Wastegate, Bleed), and FC, including SOFC, reformer, anode ejector, pre-heater and off-gas burner. The two blocks can be run separately or together, based on the simulation needs.

Like in the steady-state model, the following hypothesis were assumed:

- Air composed of nitrogen, oxygen, water, carbon dioxide and argon;
- Anodic flow including only the most significant species (methane, carbon monoxide, carbon dioxide, hydrogen, nitrogen and water);
- Equilibrium conditions for reforming and shifting reactions;
- Electrochemical reactions of carbon monoxide and methane considered negligible.

The SOFC dynamic model is based on the same equations as the steady-state model (see chapter 2.2) and the cells are discretized in 10 finite elements. The turbocharger maps are the same ones used for the steady state simulations.

It would have been too difficult to start dealing with the control of such a complex system adopting a multi input – multi output approach (control of WGV and CBV at the same time to keep both SOFC and recuperator temperatures acceptable). For this reason, in this section we focus on the control on the system varying the power load, but not the ambient temperature, which is assumed constant and equal to 15°C. Under these conditions, a single input – single output control system has been proved to be sufficient to comply with the system constraints.

A new control, acting only on the Cold Bypass valve, was tested on the steady state model, varying the current density from 100% to 60% of its design value. During these tests the Wastegate valve was always closed, while about 5% (fixed value) of the upstream mass flow was going through the Bleed valve. In Figure 22 it is possible to observe the trend of net efficiency and electrical power output in these conditions, which is similar to the previous off-design analysis.

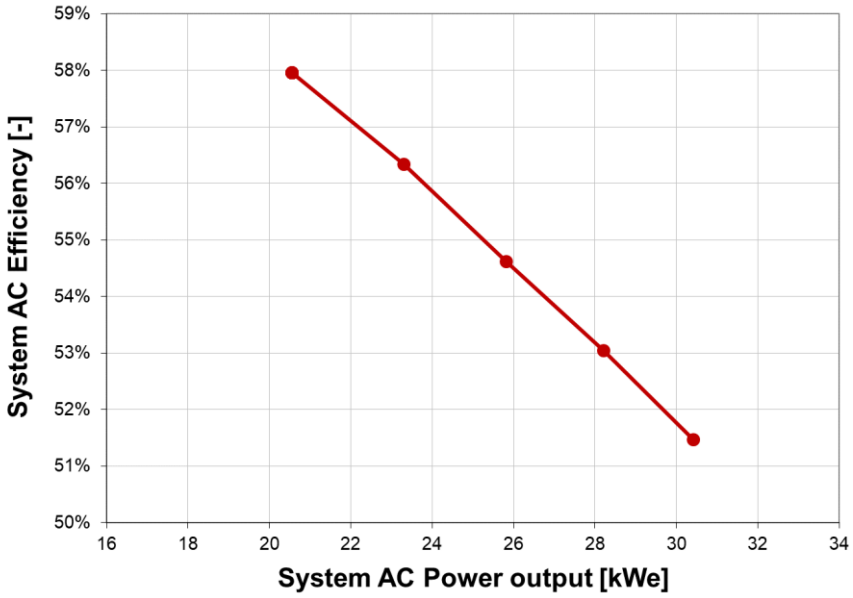

Figure 22: Global net efficiency of the system vs electrical power output at design ambient temperature (15°C), with CBV+fixed VBE control strategy

In Figure 23 it is possible to observe that, even if it is not a controlled variable, the recuperator maximum temperature is always acceptable in all the simulations.

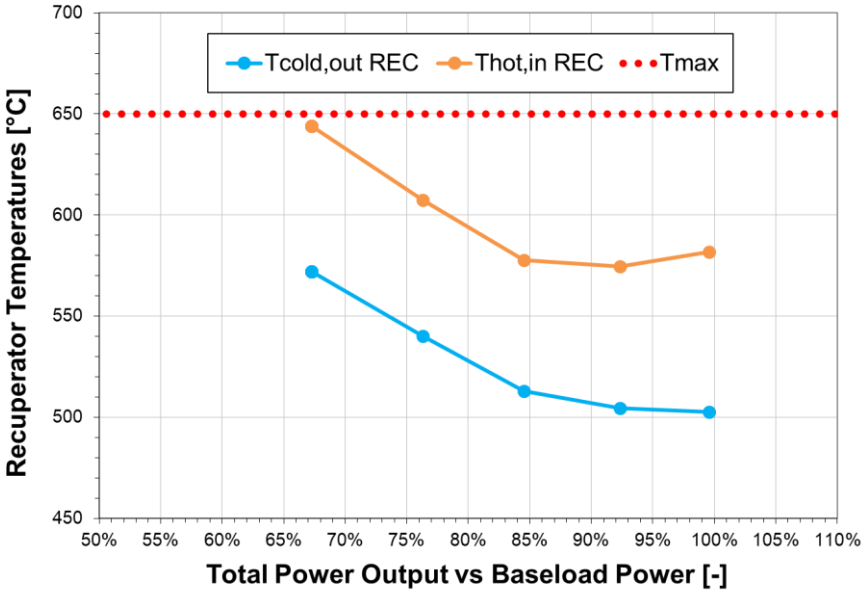

Figure 23: Recuperator temperatures vs power output percentage at design ambient temperature (15°C), with CBV+fixed VBE control strategy

The dynamic model behaviour should be as close as possible to the-steady state one, when running in steady state conditions. To do this, all the component models have been calibrated accordingly to the steady state results.

4.2 Model validation

The model of each plant component was validated against experimental data in different previous works [8][9][11][13]. Reformer and SOFC tools were validated mainly in [8] and [9]. In [8] the validation was performed comparing simulations results against experimental data collected running a Staxera GmbH system. The steady state performance of these models was validated as explained in chapter 2.3. The dynamic performance was validated in [8] on the basis of experimental data collected while varying air inlet temperature and mass flow rate, stack electrical current and fuel utilization factor (Figure 24). All the other input data have been kept constant during the experimentation.

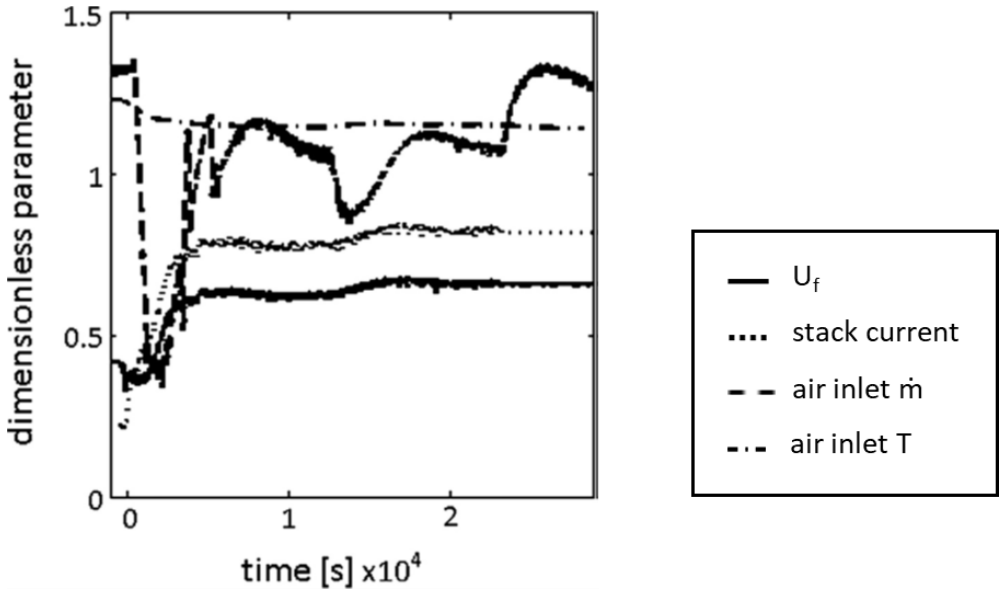

Figure 24: Input data for dynamic validation.

The validation of the SOFC is performed comparing stack voltage, solid temperature and pressure drop. The values calculated by the model match closely the experimental data for the whole period under analysis. In Figure 25 the validation of stack voltage and solid temperature trends are reported.

The pressure drop comparison, which is not reported here for the sake of brevity, can be found in [8]. The values calculated by the simulation of the model match closely the experimental data for the whole period under analysis. These results assure the reliability of the model also in dynamic conditions.

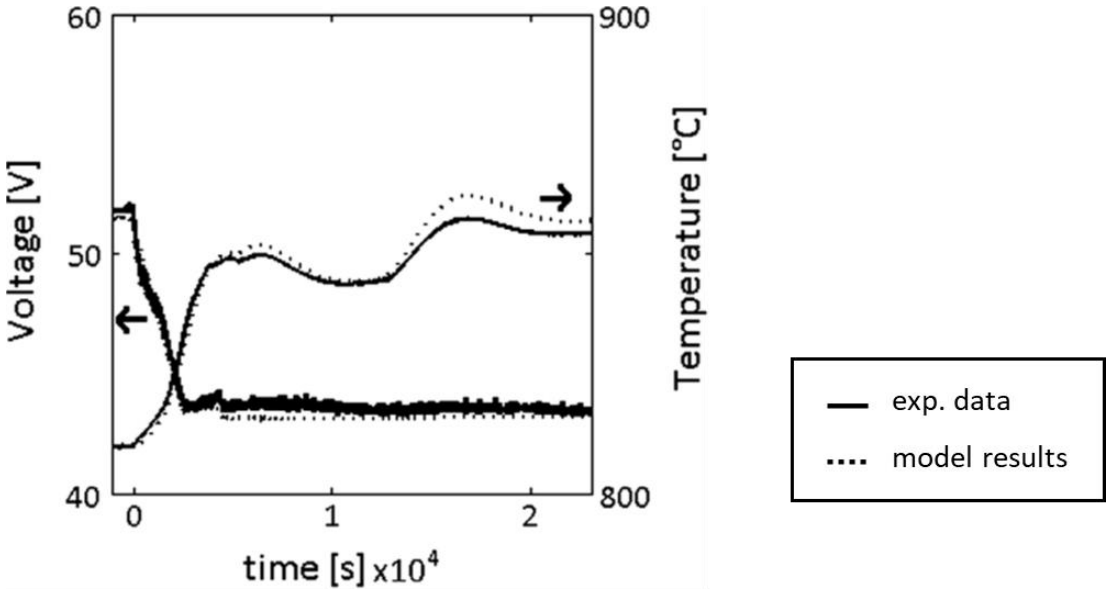

Figure 25: Stack voltage and solid temperature versus time.

Validation of the SOFC model under faulty conditions is presented and discussed in [9]. To do this, trends of temperatures, current density and power from the simulations are compared with experimental data during a reformer fault.

The reliability verification of the other plant component models was carried out in the following works: [13] for the recuperator, [11] for the ejector and D1.5 for the turbocharger devices. In [13] the recuperator is part of an externally fired micro-gas turbine system designed by Ansaldo Ricerche and the UNIGE. The validation of the transient behaviour of the recuperator model is based on experimental data collected performing power load step changes on the experimental system. In [11] an ejector based anodic test rig developed by UNIGE is presented. Many tests were run on this test rig, some concerning only the ejector, others dealing with the whole rig. For the ejector transient validation, experimental data and simulated results were compared for start-up (Figure 26) and shutdown operations (Figure 27). In both cased a good agreement between the calculated results and the experimental data was obtained.

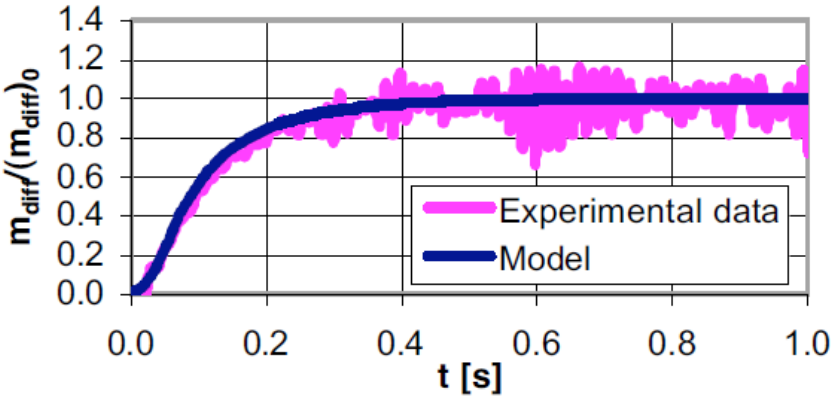

Figure 26: Ejector diffuser mass flow rate trend during start-up operation

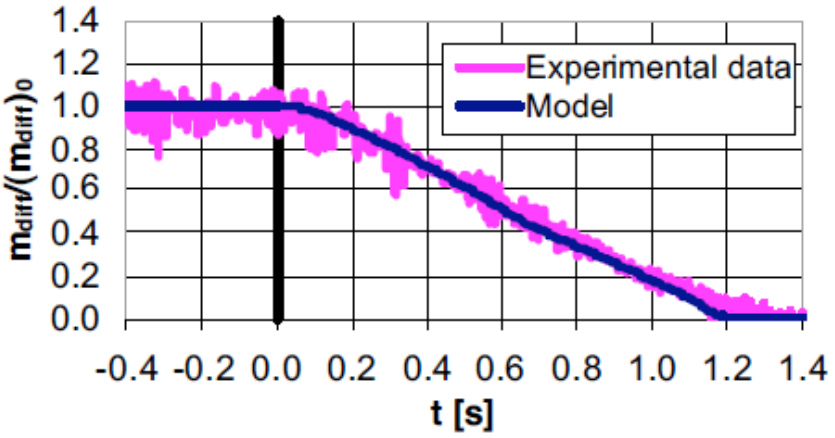

Figure 27: Ejector diffuser mass flow rate trend during shutdown operation

4.3 Results of simulations with the validated model

To study the dynamic response of the system, a CBV fractional opening step change was simulated using the dynamic model. From this simulation it was observed that the SOFC cathode outlet has a faster temperature variation than the cathode inlet, as shown in Figure 28.

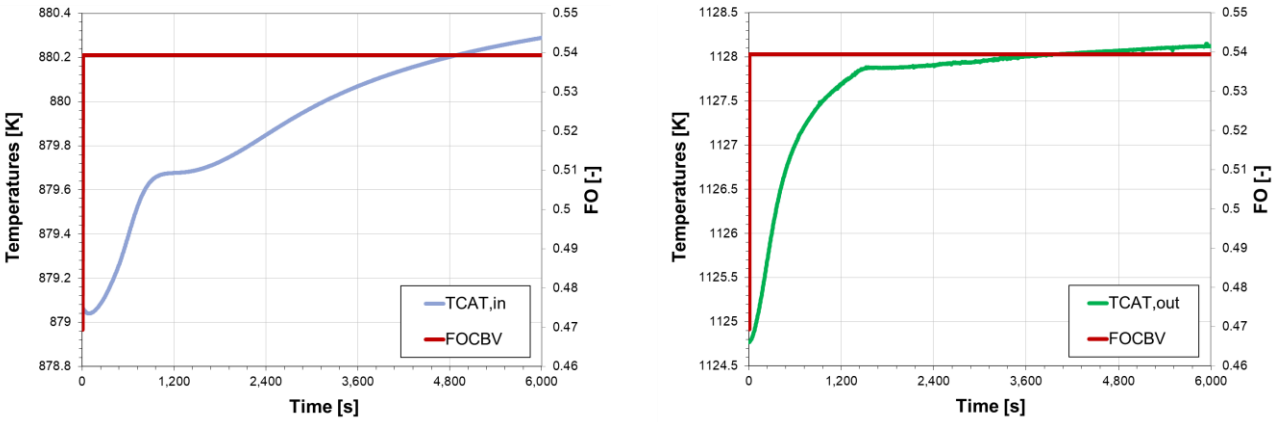

Figure 28: SOFC cathode inlet and outlet temperature variations as response to a CBV fractional opening step change

In order to have a responsive system, the control system was designed to act on the CBV fractional opening and keep the cathode outlet temperature equal to 1133 K. A PID controller was tuned on the basis of the step response simulation and a preliminary test was performed changing the current density with a ramp, from 100% to 90% of its nominal value over 500 s. During this ramp, the fuel mass flow is reduced proportionally to the current density. Figure 29 shows that the control is stable but quite slow, and the cathode outlet temperature variation is within a range of 9 K from the target value.

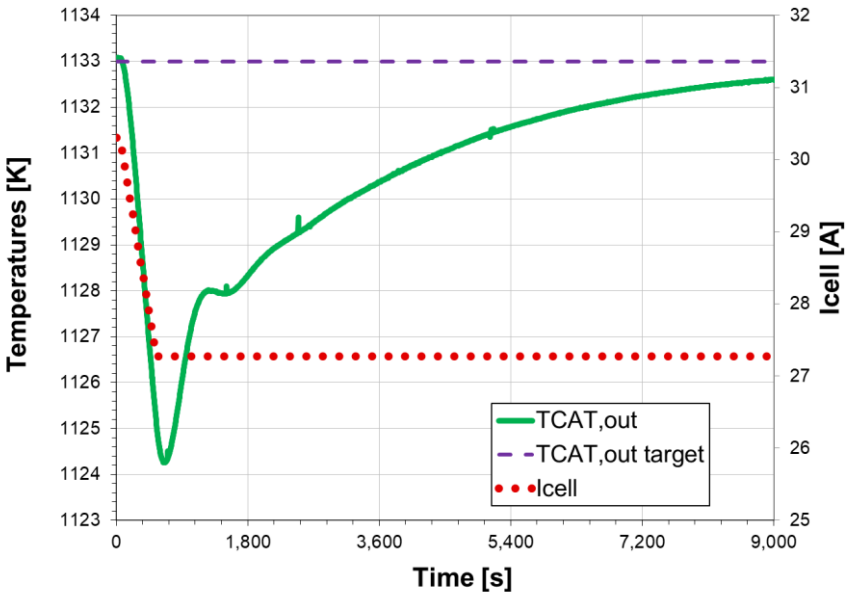

Figure 29: SOFC cathode outlet temperature variation during the current density and fuel mass flow ramp variation, with PID control strategy

With the purpose of developing a faster control system, a deeper dynamic analysis of the plant was performed. The dynamic responses of many components in the system were observed and it was noticed that the off-gas burner outlet has a faster temperature variation than the cathode outlet (Figure 30).

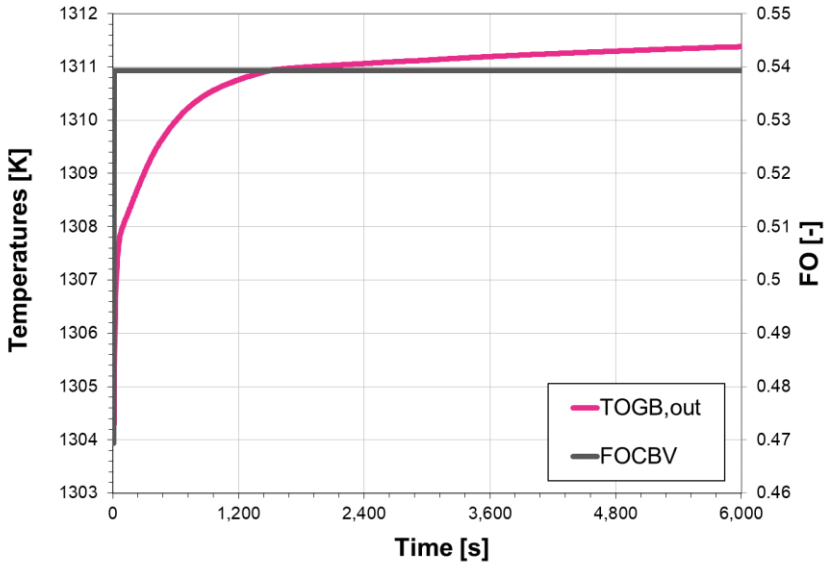

Figure 30: Off-gas burner outlet temperature variation as response to a CBV fractional opening step change

A new control was developed, combining two PIDs into a cascade control, to keep the SOFC maximum temperature equal to 1133 K. The structure of this new control system is reported in Figure 31.

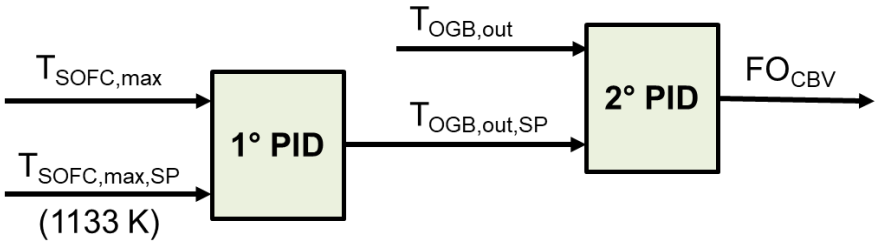

Figure 31: Cascade control acting on the CBV fractional opening to keep the SOFC maximum temperature equal to 1133K

The first PID compares the current SOFC maximum temperature with its set-point and, based on this error, it computes a temperature value, which is used as set-point of the off-gas burner outlet temperature. The second PID acts on the CBV fractional opening to decrease the difference between the off-gas burner outlet temperature and its set-point. This control

strategy was tested in the same way, changing the current density and the fuel mass flow with a ramp, from 100% to 90% of their nominal value over 500 s.

From a comparison between the old control strategy (Figure 29) and the new one (Figure 32), it is clear that the latter had the best performance. The maximum deviation from the set-point was ~7 K, against the ~9 K of the previous control strategy. Moreover, the cascade control was much more responsive: the set-point value was reached in ~1 h, while it wasn't fully reached after 2.30 h using the PID control.

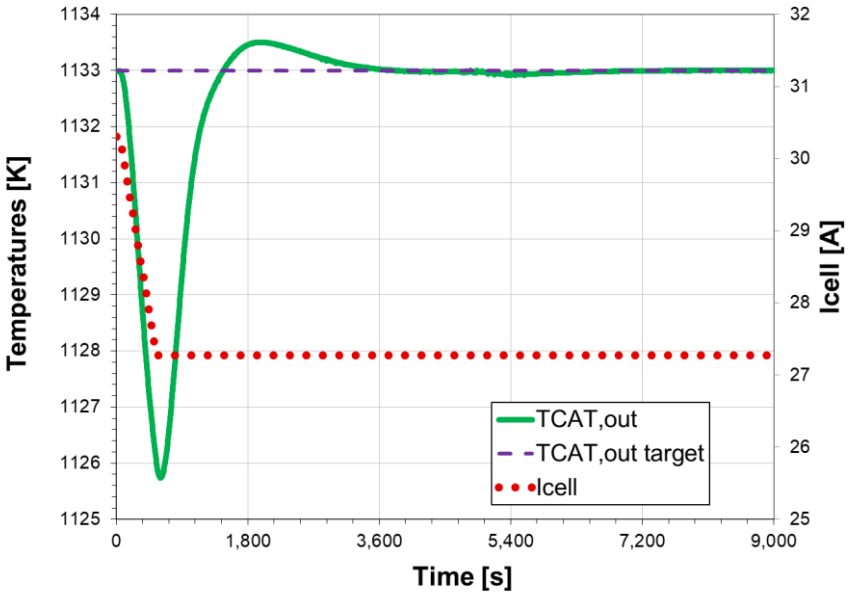

Figure 32: SOFC cathode outlet temperature variation during the current density and fuel mass flow ramp variation, with cascade control strategy

5 Real-Time Model [author: UNIGE: Mario L. Ferrari, Luca Mantelli]

In the Bio-HyPP Top-Economic Layout emulator designed by UNIGE (presented in the WP4), SOFC, air pre-heater, ejector, reformer and off-gas burner are not present, but simulated. To do this, the plant must be coupled with a real-time dynamic model in cyber-physical configuration. Fuel and air flows properties are collected by sensors on the emulator plant and used for real-time simulations. This model was developed in Matlab®-Simulink® using a library of real-time components developed at UNIGE. These models are based on the same equations and assumptions of those in the TRANSEO tool (introduced in chapter 4.1), with a few simplifications (e.g. less discretization points) in order to run the model in real-time. The real-time model is reported in Figure 33 with all the mentioned sub-blocks.

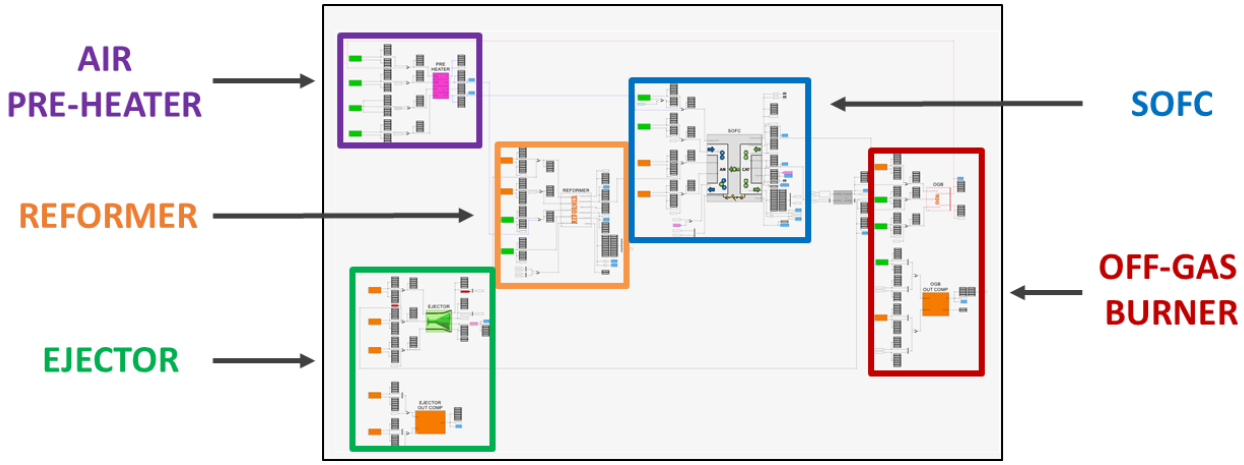

Figure 33: Matlab®-Simulink® real-time model of the Bio-HyPP Top-Economic Layout

Characteristic parameters of each component were calibrated on the basis of the steady-state and dynamic models (chapters 2.2 and 4.1 respectively). From

Table 9 it is possible to observe that the results obtained running the model in design conditions (maximum current density, ambient temperature equal to 15°C) are consistent with the steady state simulation results.

Table 9: Comparison between real-time model and steady-state model on-design simulations

		Real-Time Model	Steady-State Model
P_{el}	[kW]	32.45	32.17
V_{cell}	[V]	0.714	0.708
$T_{SOFC,max}$	[K]	1137	1133
$T_{OGB,out}$	[K]	1319	1317
$\dot{m}_{j,sec}/m_{ej,prim}$	[-]	7.03	7.10

The value of current density is set by a PID controller based on the power demand. In the steady-state simulations, it was explained how the CBV opening is controlled in different operating conditions, in order to comply with the system constraints. Modifying the valve opening, the air mass flow to the SOFC changes and, due to internal heat exchanges, its temperature changes as well. New steady-state simulations were run to collect additional data about how the air temperature changes based on current density and air mass flow. In the real-time model the CBV is not present and, to be able to simulate this effect while running the model independently from the emulator, the following procedure was adopted:

- The current density is set by a PID to match the electrical power demand;
- The air mass flow to the SOFC is determined by another PID in order to have a maximum fuel cell temperature of 1133 K;
- Current density and air mass flow are set as inputs of a look-up table to find the air flow temperature, according to the steady state simulations.

Figure 34 gives a clear explanation of this strategy.

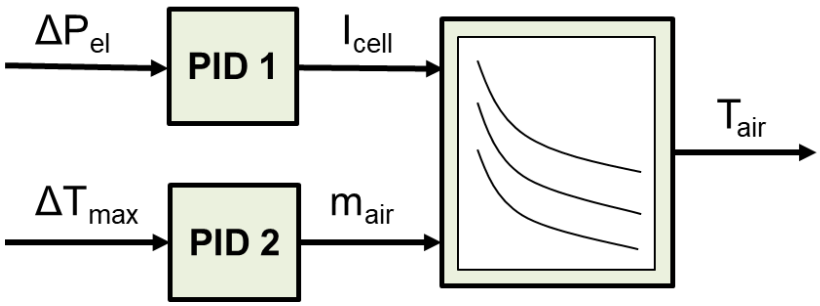

Figure 34: The control strategy adopted to compute air mass flow and temperature when running the model independently from the emulator plant

The control system was tested varying the power demand from 100% to 90% with a ramp, and back to 100% with another ramp. As shown in Figure 35 and Figure 36, the system could follow the power demand well and the maximum deviation from the target maximum SOFC temperature was always under 2.5 K.

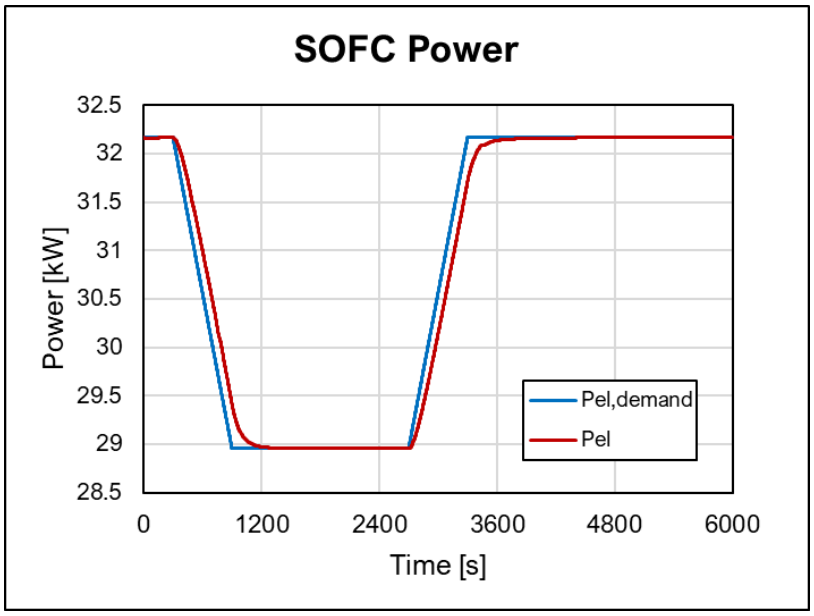

Figure 35: Comparison between power demand and actual SOFC produced power

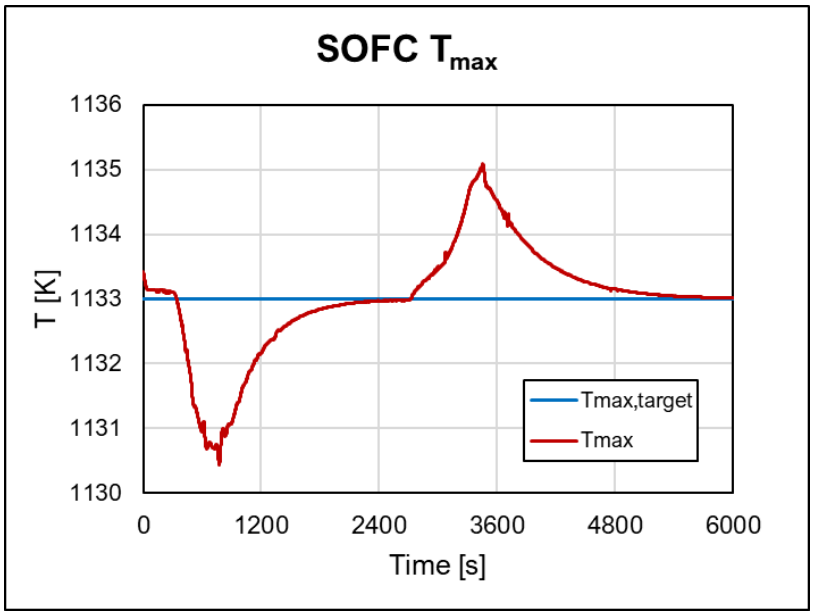

Figure 36: SOFC maximum temperature variation during the power demand variation

6 Dynamic Model of the Emulator Test Rig (Additional Activity) [author: UNIGE: Mario Ferrari]

The results obtained in the WP1 moved UNIGE to perform an additional activity (in comparison with the planned work of the Bio-HyPP project). This has been an interesting choice to have a reliable model of the emulator test rig based on a turbocharger (presented in WP4).

Being able to perform a transient analysis of the Bio-HyPP Top-Economic Layout emulator is extremely valuable to study which operations are safe and which are potentially dangerous for the plant. More specifically, it is possible to understand how to avoid:

- Overspeed of the turbocharger;
- Compressor surge;
- Exceeding temperature and pressure limits.

For this purpose, the emulator plant layout was simplified as in Figure 37, dividing the vessel in two parts (cold and hot) and considering only the bypass and bleed valves.

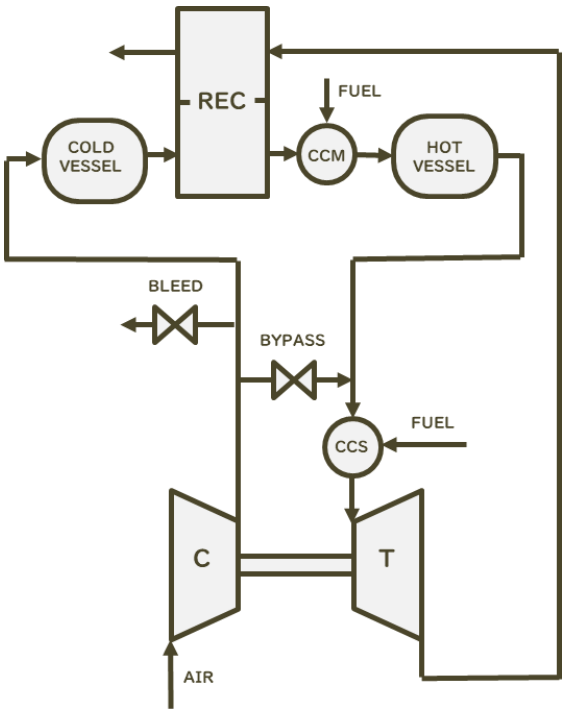

Figure 37: Simplified plant layout of the emulator plant

According to this layout, a dynamic model was developed in Matlab®-Simulink® to simulate the transient behaviour of the emulator. The component models are part of TRANSEO, a tool created at UNIGE which has already been introduced in chapter 4.1. The TRANSEO library was preferred over the real-time one (introduced in chapter 5) because this model should be used for detailed offline simulations and for not real-time applications. The characteristic parameters of the components have been calibrated on the basis of experimental data collected running tests on the plant.

The turbocharger and the emulator models have been calibrated on the basis of data collected running experimental tests (with the test rig presented in Figure 38) in steady-state conditions. The model-plant matching (see Table 10) is good with errors lower than 1.4% except for the recuperator pressure losses (cold side) that are very low values (in comparison with the probe measurement range performance).

Figure 38: Photo of the top-economic layout test rig

Table 10: Model validation in steady-state conditions

TURBOCHARGER				EMULATOR PLANT			
		Real Data	Simulation			Real Data	Simulation
N	[krpm]	1.907	1.906	$\Delta T_{REC,cold}$	[K]	421.9	427.5
β	[-]	2.3531	2.3524	$\Delta p_{REC,cold}$	[mbar]	4.8	5.1
$\dot{m}_C$	[g/s]	61.52	61.46	$T_{CCS,out}$	[K]	1320.5	1320.3
ε	[-]	2.0713	2.0081	$\dot{m}_{CBV}$	[g/s]	40.50	40.42

Figure 39 shows an example of the dynamic results obtained with this model. After 1000 s from the beginning, a 5% step in the fuel mass flow has been performed. This has generated an increase in the turbine inlet temperature and, as a consequence, in the machine rotational speed. However, since the turbocharger (operating with an air mass flow rate in the 50-60 g/s range) is connected with a 2.8 m^3 vessel, the pressurization response has required 15-20 minutes. For this reason, the rotational speed variation has involved a significant amount of time (1000-2000 s). The oscillation shown in Figure 39 is linked with the air mass flow increase due to the rotational speed increase that has decreased the turbine inlet temperature. This has generated a rotational speed decrease up to stabilization.

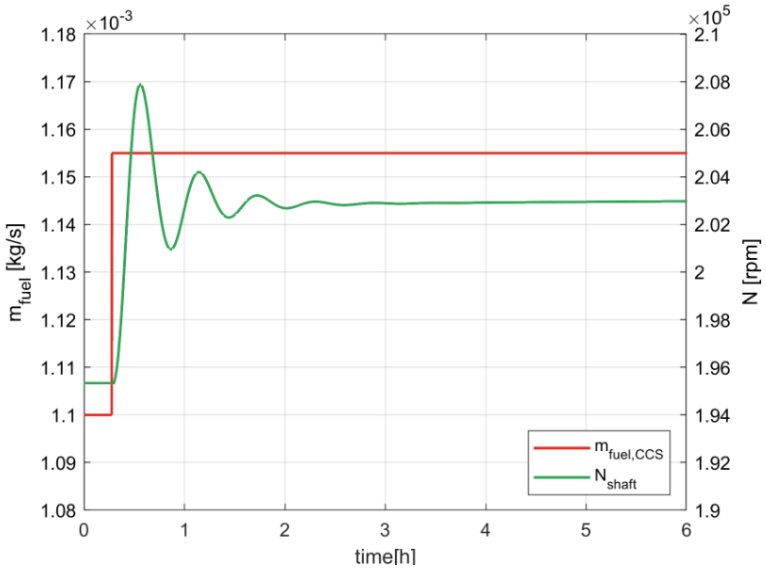

Figure 39: Model dynamic result: fuel step and rotational speed response

7 Conclusions [authors: UNIGE: Mario Ferrari, DLR: Thomas Krummrein]

UNIGE obtained these main results for the modelling activities in the Bio-HyPP project:

- The fuel flexibility analysis showed that, using an ejector designed to operate with a 50% CH_4 -50% CO_2 bio-fuel, the fuel flexibility of the system is limited. Instead, using an ejector designed to operate with a 100% CH_4 fuel, the system operative constraints are satisfied for each fuel composition in the range of 100-50% CH_4 molar fraction. The values of global power and efficiency, however, are slightly lower (2-3% decay).
- The analysis on part load conditions and ambient temperature effect demonstrated that it was possible to find a control strategy which can comply with all the Bio-HyPP Top-Economic Layout operative constraints. This control strategy acts on the opening of CBV and WGV to keep the SOFC maximum temperature at 860°C and the recuperator maximum temperature under 650°C.
- From the steady-state simulations results it was observed that the system efficiency increases lowering the power load, thanks to the reduction of losses in the SOFC. When the ambient temperature is higher, the system is more efficient thanks to the SOFC pressure increase. This effect is less significant for lower loads.
- A response surface of the Bio-HyPP Top-Economic Layout was created to evaluate the impact of some of the main operating parameters on its performance and economic profitability, considering uncertainties related to turbine and compressor efficiency and to SOFC ohmic losses. Results show that the uncertainties have a strong impact on the evaluation of the IRR, while their impact is lower on the net efficiency, and almost negligible on the net power.
- The ANOVA and the response surfaces highlighted that the current density is the most important factor for the evaluation of net power, net efficiency and IRR, as it drives directly the net power produced and so the revenues. Referring to the Italian energy market scenario, it is important to maximize the energy generation to increase the profitability of the plant.
- A transient analysis of the system was performed in dynamic conditions varying the power load and adopting a control system acting on the CBV. An additional steady-state analysis showed that this control was able to comply with all the system operative constraints.
- Varying the CBV fractional opening with a step and analysing the response of the system, it was found that the off-gas burner outlet has a faster temperature variation than the SOFC cathode outlet and inlet. A cascade control was implemented combining two PIDs in order to keep the cathode outlet temperature at 860°C, acting on the CBV.
- The cascade control was tested on a power load ramp and it gave better results than a simple PID controlling the cathode outlet temperature (set point value reached in ~1/3 of the time and smaller deviation from it during the whole ramp).

- A real-time model was developed to simulate the components that are not physically present in the emulator plant. This model was calibrated on the basis of the steady-state and dynamic analysis.
- Since the CBV is not present in the real-time model, a new control system was designed to run the model independently from the emulator, considering the effect of the valve opening on air mass flow and temperature. This control system was tested on a sequence of two load ramps and it was able to follow well the power demand and to deviate of less than 3°C from the SOFC maximum temperature set point.
- A dynamic model of the emulator test rig (additional activity in the project) was created and calibrated on the basis of experimental data. This model can be used to understand which operations are safe and which could be harmful for the plant, causing phenomena like turbocharger overspeed, compressor surge, excessively high temperatures or pressures.

DLR obtained these main results of the thermodynamic performance model of the top-performance layout:

- Measurement data is used to validate the test rigs of the DLR: the SOFC subsystem model and the components of the MGT subsystem.
- The validation of the SOFC subsystem model shows in general a good agreement with the measurement data. The simple 0D approach describes most of the parameters of the SOFC and other components in good agreement and is therefore suitable to simulate hybrid power plant steady state points in certain limits.
- The MGT subsystem main components are validated using measurement data. Turbomachinery maps are created which describe compressor flow and efficiency as well as the turbine flow with very good agreement to the measurement data. Furthermore, the pressure loss model of the combustion system and an estimation of the recuperator efficiency have been validated.

8 References

[1] Henke M., Kallo J., Friedrich K.A., Bessler W.G., Influence of Pressurisation on SOFC Performance and Durability: A Theoretical Study. FUEL CELLS 11 (2011) No. 4, 581-591.

[2] Carrero M.M., Decoupling heat and electricity production from micro gas turbines. Ph.D. Thesis, VUB, Brussels, 2018.

[3] Staunton R.H., Ozpineci B., Microturbine Power Conversion Technology Review. Oak Ridge National Laboratory, 2003.

[4] Visser W.P.J., Shakariyants S.A., Oostveen M., Development of a 3 kW Micro Turbine for CHP Applications, GT2010-22007, ASME Turbo Expo 2010, Glasgow, UK.

[5] Bernardi D., Bozzolo M., Marsano F., Tarnowski O., Agnew G., Ejectors Design in the Rolls-Royce 1 MW Hybrid System. ASME Paper 2005-GT-68085, ASME Turbo Expo 2005, Reno, Nevada (USA).

[6] Marsano F., Magistri L., Massardo A.F., Ejector performance influence on a solid oxide fuel cell anodic recirculation system. Journal of Power Sources, 129 (2004) 216-228.

[7] Costamagna P., Magistri L., Massardo A.F., Design and part-load performance of a hybrid system based on a solid oxide reactor and a micro gas turbine. Journal of Power Sources, 96 (2001) 352-368.

[8] Sorce A., Greco A., Magistri L., Costamagna P., FDI oriented modeling of an experimental SOFC system, model validation and simulation of faulty states. Applied Energy, 136 (2014) 894-908.

[9] Greco A., Sorce A., Littwin, R, Costamagna, P., Magistri L., Reformer faults in SOFC systems: Experimental and modeling analysis, and simulated fault maps. International Journal of Hydrogen Energy, 39 (2014) 21700-21713.

[10] Magistri L., Bozzo R. Costamagna P., Massardo A.F., Simplified versus Detailed SOFC Reactor Models and Influence on the Simulation of the Design Point Performance of Hybrid Systems. Journal of Engineering of Gas Turbines and Power, 126 (2004) 516-523.

[11] Ferrari M.L., Pascenti M., Massardo A.F., Ejector Model for High Temperature Fuel Cell Hybrid Systems: Experimental Validation at Steady-State and Dynamic Conditions. Journal of Fuel Cell Science and Technology, 5 (2008) 041005_1-7.

[12] D1.5 - System controls and operational envelope, Bio-HyPP project.

[13] Traverso A., Massardo A.F., Scarpellini R., Externally Fired micro-Gas Turbine: Modelling and experimental performance. Applied Thermal Engineering, 26 (2006), 1935-1941.

[14] Mantelli L., De Campo M., Ferrari M.L., Magistri L., Fuel flexibility for a turbocharged SOFC system. Energy Procedia, 158 (2019) 1974-1979.

[15] Ferrari M.L., Advanced control approach for hybrid systems based on solid oxide fuel cells. Applied Energy, 145 (2015) 364-373.

[16] James L., Dicks A., McDonald M.S., Fuel cell systems explained. Vol. 2. Chichester, UK: J. Wiley, (2003).

[17] Traverso A., TRANSEO code for the dynamic performance simulation of micro gas turbine cycles. ASME Turbo Expo 2005: Power for Land, Sea, and Air. American Society of Mechanical Engineers Digital Collection (2005).

[18] Magistri L., Costamagna P., Traverso A., Ferrari M.L., Massardo A.F., Transient Analysis of Solid Oxide Fuel Cell Hybrids. Part C: Cycle Model, ASME Paper 2004-GT-53845, ASME Turbo Expo (2004).

[19] Pilidis P., Maccallum N.R.L., A General Program for the Prediction of the Transient Performance of Gas Turbines, ASME Paper 85-GT-265 (1985).
[20] Garrard G., ATEC: The Aerodynamic Turbine Engine Code for the Analysis of Transient and Dynamic Gas Turbine Engine System Operations, Part 1: Model Development, ASME paper 96-GT-193 (1996).
[21] Bozzi L., Dynamic Modular Simulation of Power Generation Plants, Ph.D. Thesis, DiMSET, Università di Genova, Genova, Italy (2003).
[22] Giugno A., Mantelli L., Cuneo A., Traverso A., Robust Design of a Hybrid Energy System. E3S Web Conf. 113 02008 (2019), DOI: 10.1051/e3sconf/201911302008.
[23] Cuneo A., Zaccaria V., Tucker D., Traverso A., Probabilistic analysis of a fuel cell degradation model for solid oxide fuel cell and gas turbine hybrid systems. Energy, 141 (2017) 2277-2287.
[24] Arsalis A., Thermoeconomic Modeling and Parametric Study of Hybrid SOFC-Gas Turbine-Steam Turbine Power Plants Ranging from 1.5 to 10 MWe. J. Power Sources, 181 (2008) 313–326.
[25] Galanti L., Massardo A. F., 2011, Micro Gas Turbine Thermodynamic and Economic Analysis up to 500 KWe Size. Appl. Energy, 88 (2011) 4795–4802.
[26] M. Herbst, M. Hohloch, M. Metten, D4.5 Lessons learned for development, set-up and installation of a hybrid power plant demonstrator, public deliverable, Bio-HyPP project, 2019
[27] T. Krummrein, D1.2 Static thermodynamic system models, public deliverable, Bio-HyPP project, 2019
[28] M. Henke, M. Steilen, C. Schnegelberger, M. Riedel, M. Hohloch, S. Bücheler, M. Herbst, A. Huber J. Kallo, K.A. Friedrich, Construction of a 30kW SOFC Gas Turbine Hybrid Power Plant, ECS Transactions, 68.1, page 85-88, (2015).
[29] M. Steilen, Thermodynamic modeling and experimental investigation of operating conditions for a SOFC/GT hybrid power plant, Ph.D. Thesis, University of Stuttgart, 2019
[30] M. Tomberg, D2.5 SOFC Auxiliary component characterization, public deliverable, Bio-HyPP project, 2017
[31] Srikanth S., M.P. Heddrich, S. Gupta, K.A. Friedrich, Transient reversible solid oxide cell reactor operation - Experimentally validated modeling and analysis, Applied Energy, 2018
[32] M. Bolemant, D. Peitsch, An alternative compressor modeling method with gas turbine performance simulations, DGLR, 340047, 2014
[33] F. Payri, J.R. Serrano, P. Fajardo, M.A. Reyes-Belmonte, R. Gozalbo-Belles, A physically based method to extrapolate performance maps of radial turbines, Energy Conversion and Management 55, 2012
[34] M. Henke, T. Monz, M. Aigner, Inverted Brayton cycle with exhaust gas recirculation – a numerical investigation, Journal of Engineering for Gas Turbines and Power, 2013